ELSEVIER

Contents lists available at ScienceDirect

# Construction and Building Materials

journal homepage: www.elsevier.com/locate/conbuildmat



# Influence of limestone filler on potassium citrate activated BOF slag binder

S. Yvars <sup>a,\*</sup> , K. Schollbach <sup>a</sup> , T. Wattez <sup>b</sup>, S. Van der Laan <sup>a</sup>, H.J.H. Brouwers <sup>a</sup>

### ARTICLE INFO

Keywords:
BOF slag
Fine fillers
Potassium citrate
Hydration kinetic
Mechanical performance
Phase assemblage

### ABSTRACT

Basic Oxygen Furnace slag (BOF slag) is a by-product of steelmaking, which is mainly composed of  $C_2S$  and Brownmillerite ( $C_4$  (A, F), which give it cementitious properties. Previous work reveals that citrate salts can activate Brownmillerite to obtain a performant binder based on BOF slag without including any Portland cement. Nevertheless, the  $C_2S$  is still not activated in this system, and its early reactivity remains very low. The effect of limestone on the mechanical properties of the binder and its phase assemblage are investigated and compared to the effect of quartz. The results show that the use of fillers improves the performances of the BOF slag pastes with more hydration products being formed. They highlight the superior effect of fine limestone incorporation, compared to quartz, with a minimum dosage of 9 vol%. The resulting BOF slag binder exhibits an increase in compressive strength of 55 % compared to the reference and a decreased total porosity.

# 1. Introduction

Cement is the world's most widely produced building material but comes at a significant environmental cost, contributing to 5-10 % of global  $CO_2$  emissions [1–3]. Addressing this ecological challenge necessitates innovative approaches, and one highly effective strategy involves the development of new low-carbon binders and concretes that incorporate waste or industrial by-products [4–8].

Among such by-products, Basic Oxygen Furnace (BOF) slag, a material produced during the refinement of iron ore into steel [9], exhibits hydraulic properties. It is abundant (approximately 100 kg per ton of steel) [10-13] and largely landfilled or used for low-end applications, leading to landfills and contamination of the waters and soils with heavy metals. Moreover, volume instability is frequently reported as a major challenge when using BOF slag in applications as aggregate. The reaction of free lime (f-CaO) with water to form portlandite (Ca(OH)2) leads to a substantial volume increase due to the difference in specific density between the two phases. Similarly, free periclase (f-MgO) may also contribute to expansion. However, f-MgO is generally absent in BOF slag, as magnesium is mainly incorporated into the wuestite (Fe,Mg)O solid solution. While a high content of free lime may indeed cause expansion even in fine powders, some BOF slags that contain extremely low or undetectable amounts of f-CaO [12,14], generate growing interest in their use as cementitious binders [13,15–19].

BOF slag is typically composed of CaO (30-50 %), Fe<sub>2</sub>O<sub>3</sub> (20-40 %),

Nevertheless, in this system, the degree of hydration of  $C_2S$  remains relatively low [12,19].  $C_2S$  is the primary component of BOF slag, and it is known to incorporate phosphate as well as vanadium, stabilizing the different polymorphs of  $C_2S$  present in the material,  $\beta$ - $C_2S$ ,  $\alpha$ '- $C_2S$ , [24, 25] and reducing its reactivity. Its delayed reactivity limits the formation of calcium silicate hydrates (C-S-H), which are fundamental to the development of mechanical strength, durability, and overall performance of the binder. Therefore, this study focuses on improving the reactivity of  $C_2S$  by adding mineral fillers to BOF slag pastes. And, more

E-mail address: s.r.yvars@tue.nl (S. Yvars).

<sup>&</sup>lt;sup>a</sup> Department of the Built Environment, Eindhoven University of Technology, P.O. Box 513, Eindhoven, MB 5600, the Netherlands

<sup>&</sup>lt;sup>b</sup> Ecocem Materials Ltd, 4 Place Louis Armand, Paris 75012, France

 $SiO_2$  (10–20 %), MgO (4–10 %),  $Al_2O_3$  (1–7 %),  $P_2O_5$  (1–3 %), MnO (0-4 %), and  $TiO_2$  (0-2 %). It should be noted that BOF slag contains both divalent and trivalent iron at a variable ratio. BOF slag contains the minerals: β-C<sub>2</sub>S, α'-C<sub>2</sub>S, C<sub>4</sub>(A, F), C<sub>2</sub>F, and RO phase (CaO-FeO-MgO-MnO solid solutions), [20,21]. It can also contain small amounts of free lime and C<sub>3</sub>S. Although BOF slag initially shows very low hydraulic activity [12] especially due to the poor early reactivity of C2S [22,23], it demonstrates great performance while adequately activated [17–19]. A prior study demonstrated that adding tri-potassium citrate to BOF slag paste leads to a highly performant binder without including any cement. achieving up to 75 MPa after 28 days of hydration. This activator significantly reduces the water demand of the paste, enabling the use of very low water-to-binder (w/b) ratios while maintaining good flowability without the need for superplasticizers. In addition, it promotes the dissolution of brownmillerite, leading to an increase in the early compressive strength [18].

<sup>\*</sup> Corresponding author.

generally, on investigating the unknown impact of fillers on the hydration of potassium citrate-activated BOF slag binder.

The use of fillers is known to improve the reactivity of clinker phases in Ordinary Portland Cement (OPC) [26,27]. Incorporating fillers will modify several parameters in the system. Firstly, fillers may help fill the voids between particles, effectively reducing the inter-particle distance. This packing optimization intensifies the shearing of the particles, promoting the dissolution of ions into the pore solution. The filler can also act as nucleation sites, supporting the formation of C-S-H during the  $C_2S$  hydration, acting on the number of nuclei and their growth [28].

However, it is important to note that the choice of the filler is critical and can significantly change the impact and the final properties of the binder. Parameters such as particle size distribution (PSD), specific surface area (SSA), dosage, and the chemical nature of the filler should be considered. Limestone powder, for instance, has shown a favourable effect in Ordinary Portland Cement (OPC) based systems, enhancing the formation of C-S-H gel more than other fillers like quartz, as it directly acts on the  $C_3S$  dissolution [29]. Overall, the smaller the PSD and the higher the SSA, the better the effect of fillers. In the case of limestone filler addition, notable effects are observed with up to 5 wt% replacement [30,31], with apparent adverse effects when this amount exceeds 10-15% per cement mass while maintaining a constant water-to-powder ratio [31].

In this study, limestone or quartz fillers are incorporated into a BOF slag activated with 1 wt% tri-potassium citrate, whilst varying the size and the SSA (coarse and fine fillers) and the volume substitution (3, 6, and 9 vol%). The influence of these fillers on the hydration kinetic, the mechanical properties, and the microstructure of the binder after 7, 28, and 56 days of curing, is investigated by combining calorimetry and strength tests with thermogravimetry (TG), quantitative XRD, and Mercury Intrusion Porosimetry (MIP).

# 2. Methodology

The water demand of each filler individually was characterized by performing the Punkte test [32]. The testing procedure consists of weighing the amount of water added to a powder until the first signs of bleeding appear. At this saturation point, the following equation is used to determine the water demand  $\Phi$ . It is assumed that the system is then free of air, and all voids are filled with water.

$$\Phi = \frac{V_W}{V_p + V_w} = \frac{m_w}{m_w + m_p * \rho_p / \rho_w}$$
 (1)

Where V, m and  $\rho$  are the volume, the mass and the density of the water (w) or the powder (p).

The density of each raw material was determined with a Helium pycnometer (AccuPyc II 1340) on material dried in an oven for 24 h at  $40^{\circ}$ C.

The hydration kinetics of the pastes were investigated by isothermal calorimetry (I-cal ultra, Calmetrix), at 20  $^{\circ}$ C. Tri-potassium citrate was first dissolved in water to obtain a solution of 0.19 M. The powder material, including BOF slag and the chosen amount of filler (0, 3, 6, 9 vol%) were inserted in plastic ampoules and mixed for 1 min. Then, the tri-potassium solution was added, with a chosen solution to powder ratio (w/p) of 0.18. The resulting paste was mixed for 2 min. After 45 min needed to have a completely stable voltage in the calorimeter, each sample was loaded into the machine. The heat flow and the cumulative heat were measured for 3 days.

Cubic paste samples (4x4x4 cm³) were mixed, cast and cured accordingly to standard procedure EN 196–1:2005. Each sample was prepared in 3 replicates and cured for 7, 28, and 56 days in a sealed box containing water to create a humid environment and placed at ambient temperature. The samples were placed on a grid to avoid direct contact with the water in the box. After testing the compressive strength of the samples, the cubes were crushed with a hammer and sieved to obtain 2

different-size fractions, one finer than 200  $\mu m$  and one between 2 and 4 mm. The fine powder was used to perform TG and XRD, while the coarse fraction was used for MIP measurements. The hydration of each fraction was stopped separately by removing the remaining free water using the double solvent exchange method [33]. The samples were, first, immersed in isopropanol for 10 min to remove all the free water and then vacuum filtered and dried with diethyl ether. Each sample was carefully stored, in sealed containers, avoiding air contact to prevent carbonation.

The porosity and the pore structure of the samples, after 28 and 56 days of hydration, were characterized by performing Mercury Intrusion Porosimetry (MIP) using the 2–4 mm fraction samples. The measurements are conducted with an Autopore IV 9500 with a pressure varying from 0 to 228 MPa, a contact angle of 130, and a mercury surface tension of 485 dynes/cm.

Thermogravimetry analysis (TGA) is performed to assess the differences in the hydrate assemblage. Around 100 mg of powder is used. The results are recorded by a Netzsch simultaneous analyser (STA 449 C) with a heating rate of 20  $^{\circ}$ C/min, from a temperature of 40 $^{\circ}$ C to 1000  $^{\circ}$ C under a nitrogen atmosphere.

The chemical composition of the raw materials is measured with X-ray fluorescence spectroscopy with an XRF spectrometer from PAN-alytical (Epsilon 3 range, standardless OMIAN method), on fused beads samples. Additionally, free lime (f-CaO) amount in the raw slag was determined by hot ethylene-glycol extraction (1 g sample, heated at 80°C, under reflux for 30 min) followed by titration with hydrochloric acid (0.1 N) to a phenolphthalein endpoint [34–37]. The content was calculated as:

$$\%fCaO = \frac{V_{HCl} \times N_{HCl} \times M_{CaO}}{2 \times m_{BOF} \times 1000} \tag{2}$$

Where  $V_{HCl}$  is the titrant volume (mL),  $N_{HCl}$  its normality,  $M_{CaO}$  the molar mass of CaO, and  $m_{BOF}$  the sample mass (g).

Periclase (f-MgO) content was measured by ammonium nitrate extraction (1 g sample, heated at 85°C under reflux, for 2 h) and subsequent complexometric titration with EDTA. The titrated solution was buffered at pH 10 and the titration was monitored using a pH meter [35, 38]. The content was calculated as:

$$\%fMgO = \frac{V_{EDTA} \times C_{EDTA} \times M_{MgO}}{m_{BOF} \times 1000}$$
(3)

Where  $V_{EDTA}$  is the titrant volume (mL),  $C_{EDTA}$  its molar concentration,  $M_{MgO}$  the molar mass of MgO, and  $m_{BOF}$  the sample mass (g).

The mineralogical composition of the raw materials and the hydrated pastes is determined with Q-XRD. The samples are prepared by intermixing powders and around 10 wt% silica internal standards in an XRD-Mill McCrone (RETSCH) and backloading them into sample holders. The diffraction patterns were determined with a D4 ENDEAVOR X-ray Diffractometer with Co radiation ( $\lambda$ =1.79 Å), a voltage of 40 kV, and a current of 40 mA. Samples were measured using a step size of 0.014 $\circ$  20 and a time per step of 1 s for a 20 range of 12–80 $\circ$  20. The hydrate and remaining phase amounts were quantified with TOPAS Academic software v5.0, using the Rietveld method [39]. The refined parameters used for the quantification were the crystallite size, the lattice parameters, the zero error, and the background. The structural data of the phases used for the quantification can be found in Table A1, in Appendix.

Two-way Analysis of Variance (ANOVA) performed with Origin software, was used to evaluate the influence of the different parameters and their interaction on the measured properties of the slag pastes. The analysis was performed considering four independent parameters: (A) age of the samples (7, 28, or 56 days); (B) filler nature (quartz or limestone); (C) filler size (coarse or fine); (D) filler dosage (0, 3, 6 or 9 vol%). Combinations of two parameters were tested to determine their individual and interactive effects on four chosen variable responses: (1)

Compressive strength; (2) Total porosity; (3) Hydration product amount (XRD); (4) Mass loss (TGA). The statistical significance was assessed at a 95 % confidence level (p < 0.05).

### 3. Materials

The BOF slag used in this study was provided by Tata Steel IJmuiden (The Netherlands) and milled for 20 min in a vibratory disc mill (RS 300, Retsch) resulting in a material  $d_{50}$  of 12.3  $\mu$ m. Two different batches of quartz filler were obtained by milling sand in the same disc mill for 15 min and 30 min, respectively to obtain one coarse quartz (CQ) fraction with a  $d_{50}$  of 10.5  $\mu$ m and a finer quartz (FQ) with a  $d_{50}$  of 4.3  $\mu$ m. In the same way, two limestone fillers of different fineness, produced by Omya (France), were used, one coarse (CL) and one fine (FL) with respective  $d_{50}$  of 10.0 and 4.4  $\mu$ m. The particle size distribution (PSD) of each raw material was measured by laser diffraction spectroscopy (Mastersizer 2000, Malvern) in isopropanol as shown in Fig. 1. The Specific Surface Area (SSA) and the water demand of the fillers were respectively determined by performing BET analysis and the Punkte test (described in Section 2.3.1) and are reported in Table 1.

The individual material chemical and mineralogical compositions were characterized with X-ray fluorescence and quantitative X-ray diffraction spectroscopy. The results are shown in Table 2 and Table 3, respectively. The free lime (f-CaO) content was determined by chemical extraction and acid titration and found to be 0.28 %, corresponding to 1 mL of HCl (0.1 N) required for the phenolphthalein endpoint. Free MgO (periclase) was below the detection limit of the ammonium chloride extraction, EDTA titration method, as no inflection was observed in the potentiometric titration curve.

# 4. Mix design

The effect of limestone addition in tri-potassium citrate activated BOF slag pastes is studied and compared to quartz filler, which is known to be less effective in OPC systems. Two different sizes and four dosages are tested, based on preliminary experiments and the literature [29,42] to investigate the effect of the amount, and the PSD/SSA of the fillers on the binder properties. The fine limestone, coarse limestone, fine quartz, and the coarse quartz are named FL, CL, FQ and CQ, respectively. The filler amounts chosen for this study are 0, 3, 6, and 9 vol%. For instance, FL6 contains 6 vol% of fine limestone. A citrate solution to powder ratio (w/p) of 0.18 was chosen to obtain good and comparable workability with the addition of filler and avoid bleeding of the paste. The addition of tri-potassium citrate enables to reach a very good workability without the addition of superplasticizers. The citrate solution of 0.19 M was prepared to make the amount of tri-potassium citrate correspond to 1 wt % of the mass of solid materials based on the recommendations of [18,

**Table 1**Physical properties of the raw materials.

	Material	Skeleton density (g/cm <sup>3</sup> ) <sup>a</sup>	d <sub>50</sub> (μm)	SSA (m²/g)	Water demand <sup>b</sup>
BOFs	BOF slag	3.85	12.26	1.06	-
FL	Fine	2.54	4.42	2.09	0.368
	limestone				
CL	Coarse	2.54	10.02	0.66	0.316
	limestone				
FQ	Fine quartz	2.55	4.34	5.13	0.374
CQ	Coarse quartz	2.56	10.51	3.21	0.358

<sup>&</sup>lt;sup>a</sup> Measured by helium pycnometry

**Table 2**Oxide composition of the raw materials as determined with XRF.

	BOF slag	Fine limestone	Coarse Limestone	Quartz
Oxide	Content (wt %)	Content (wt %)	Content (wt%)	Content (wt %)
CaO	41.3	69.1	69.2	-
FeO/	31.0	0.1	0.0	3.4
$Fe_2O_3^a$				
$SiO_2$	10.9	0.3	0.2	94.1
MgO	5.3	-	0.1	-
MnO	5.3	0.1	-	0.0
$Al_2O_3$	1.5	0.2	-	2.1
$TiO_2$	1.4	-	-	-
$V_2O_5$	1.1	-	-	-
$P_2O_5$	1.0	-	-	-
$Cr_2O_3$	0.3	-	0.0	0.4
SrO	-	0.0	0.0	-
$LOI_{p}$	$-0.9^{c}$	30.3	30.5	0
f-CaO	0.28	-	-	-
f-MgO	0	-	-	-

 $<sup>^{\</sup>rm a}$  BOF slag contains iron with different oxidation states. The Fe3 + /Fe total ratio may vary for different batches but was estimated at around 0.25 by Zepper et al. [40]

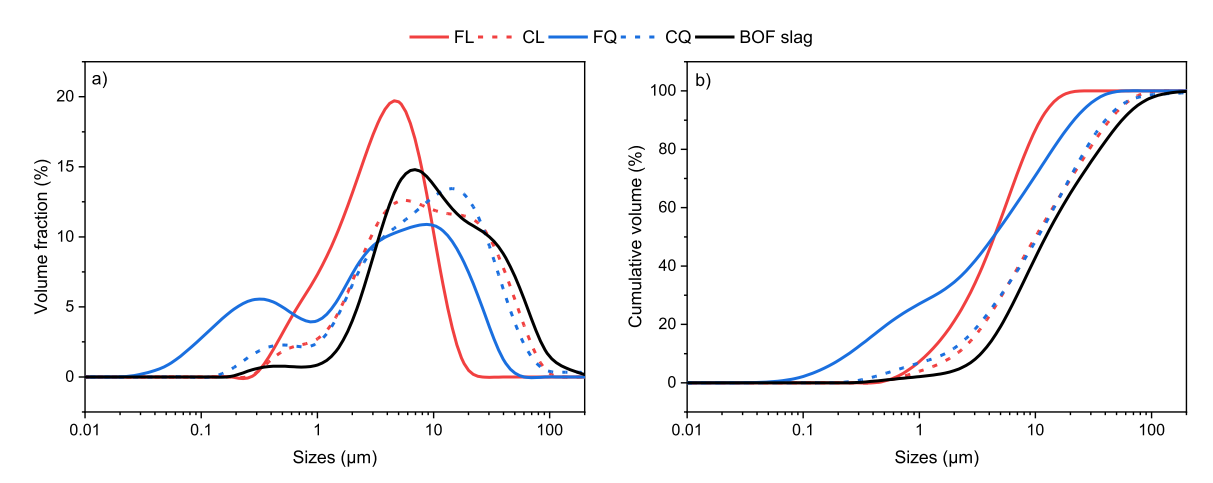


Fig. 1. PSD of the raw materials measured by laser diffraction spectroscopy in isopropanol, (a) Volume percentages; b) Cumulative volume percentages).

<sup>&</sup>lt;sup>b</sup> Values determined by Punkte Test (described in the method section)

<sup>&</sup>lt;sup>b</sup> Loss on ignition corresponds to the weight of volatile compounds

<sup>&</sup>lt;sup>c</sup> Negative LOI corresponds to a gain on ignition representing an increase in mass rather than a decrease after heating the sample at 1000°C. For BOF Slag this increase might be attributed to an increase in the overall mass due to the oxidation of iron contained in large quantities [18,40,41]

**Table 3**Quantitative phase composition (wt%) of the raw materials.

Phase (wt%)		BOF slag	Quartz	Limestone
Brownmillerite	Ca <sub>2</sub> (Al,Fe) <sub>2</sub> O <sub>5</sub>	16.7	-	-
C <sub>2</sub> S	Ca <sub>2</sub> SiO <sub>4</sub>	40.0	-	-
Wuestite	(Mg,(Fe)O)	18.4	-	-
Magnetite	Fe <sub>3</sub> O <sub>4</sub>	6.3	-	-
Lime	f-CaO	0.4	-	-
Calcite	CaCO <sub>3</sub>	0.7	-	84.9
Quartz	$SiO_2$	-	71.3	2.5
Iron	Fe	-	1.3	
Amorphous	-	18.6	27.5	12.6

Table 4 Mix design.

Volume replacement	Mass replacement	Filler (g)	BOFs (g)	Solid (g)	w/p <sup>a</sup> ratio	w/ <sup>b</sup> ratiob
0 %	0 %	0	250	250	0.18	0.180
3 %	2.01 %	5.03	244.97	250	0.18	0.184
6 %	4.06 %	10.15	239.85	250	0.18	0.188
9 %	6.15 %	15.38	234.62	250	0.18	0.192

 $<sup>^{\</sup>rm a}$  w/p ratio refers to the mass of citrate solution (0.19 M) per mass of powder material including fillers and BOF slag.

19]. The composition of all the mixes is summarized in Table 4.

# 5. Results and discussions

### 5.1. Hydration kinetics

The hydration reaction of BOF slag pastes containing different types and amounts of filler was investigated by isothermal calorimetry. The results are normalized by the weight of BOF slag and plotted in Fig. 2. A distinct peak attributed to brownmillerite hydration and hydrogarnet formation, promoted by tri-potassium citrate [43,44] is observed for all the samples. In the case of limestone addition, the maximum hydration peak occurs almost at the same time as for the reference. No significant differences are observed regarding the fineness or the amount of limestone filler. On the other hand, the incorporation of quartz filler appears to extend the induction period and therefore delay the appearance of the main hydration peak. Interestingly this effect is also not in correlation with the filler size or amount. The total heat released for all samples is between 65 J/g and 70 J/g after 60 h. However, an accelerating effect of limestone filler would have been expected, as commonly observed in OPC systems [28,45–47]. The delay observed for the quartz samples could be attributed to an increase in the effective water-to-binder (w/b) ratio with increasing filler dosage, given that the water-to-powder (w/p) ratio remained constant at 0.18 for all the samples (Table 4). This can extend the time before the pore solution reaches saturation and hydration products start to precipitate, resulting in a prolonged induction period and a delay of the main hydration peak. In this case, it is conceivable that limestone accelerates hydration, therefore compensating for the dilution effect.

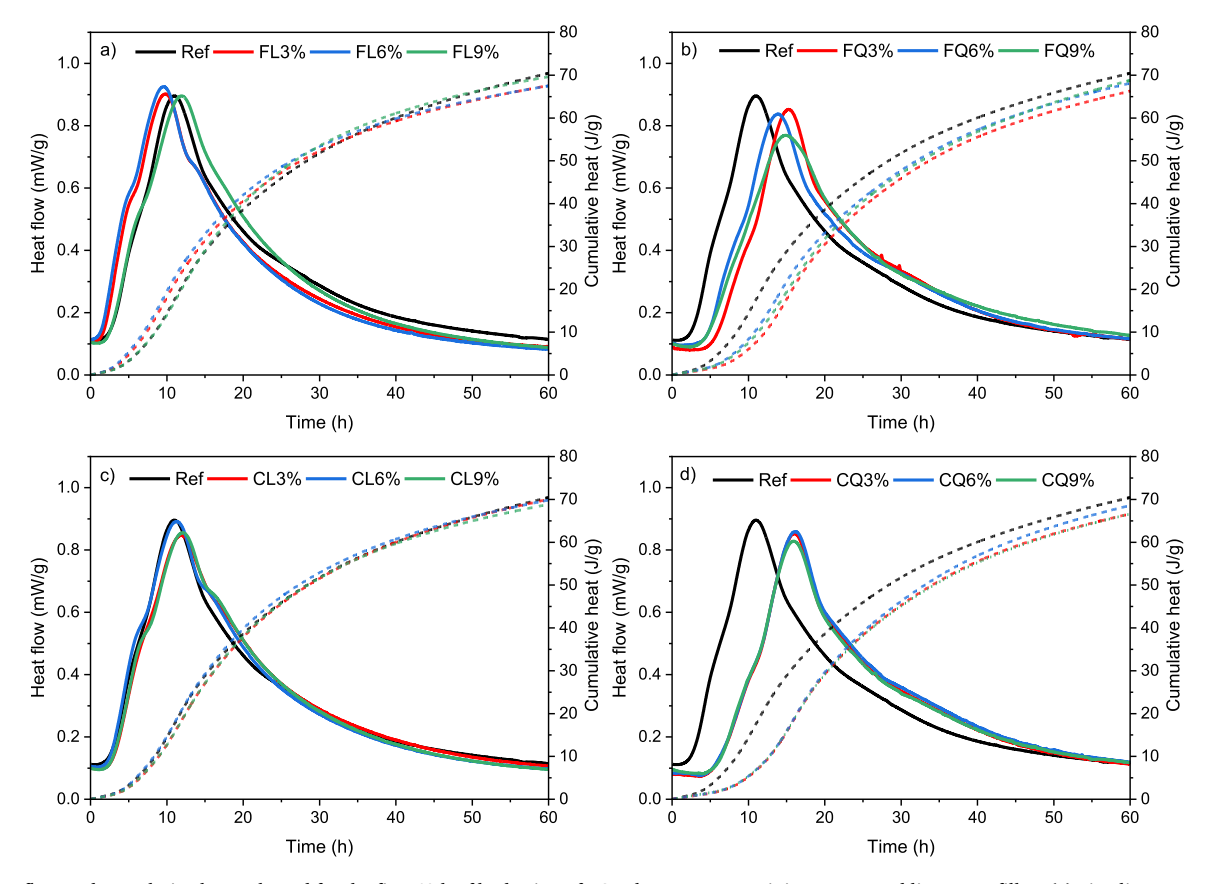


Fig. 2. Heat flow and cumulative heat released for the first 60 h of hydration of BOF slag pastes containing quartz and limestone fillers (a) Fine limestone samples; b) Fine quartz samples; c) Coarse limestone samples; d) Coarse quartz samples).

<sup>&</sup>lt;sup>b</sup> w/b ratio excludes the presence of filler and is only based on the amount of citrate solution per weight of BOF slag – the w/b increases with the filler amount as the BOF slag percentage is lower.

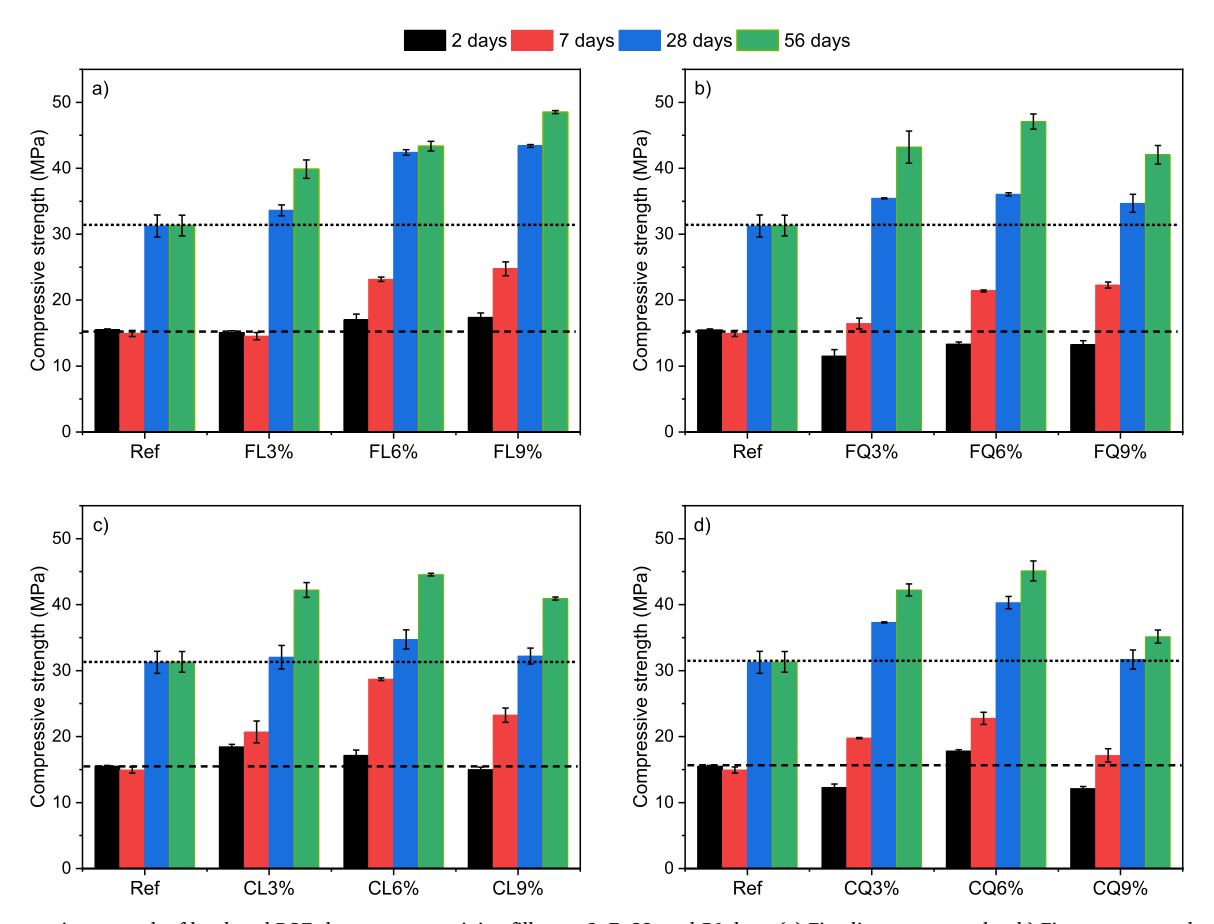


Fig. 3. Compressive strength of hardened BOF slag pastes containing fillers at 2, 7, 28, and 56 days, (a) Fine limestone samples; b) Fine quartz samples; c) Coarse limestone samples; d) Coarse quartz samples).

# 5.2. Mechanical performances

The compressive strength of the mixes was measured at 2, 7, 28, and 56 days and is reported in Fig. 3. At a very early age, no effect of the filler addition is observed, and the compressive strength of all the samples is around 15 MPa. However, from 7 days up to 56 days, the addition of filler leads to an increase in compressive strength compared to the reference, which gives at each age the lowest values of 14.9, 31.25, and 31.3 MPa. The general trend indicates a more favourable impact of coarse fillers before 28 days of curing, while the highest strength values at 56 days are achieved with the inclusion of fine fillers. Specifically, pastes containing CL filler demonstrate higher compressive strength at 7 days (for instance 28.7 MPa for CL6, against 24.7 MPa for FL9), whereas the incorporation of FL leads to greater improvement at 28 and 56 days (43.4 and 48.5 MPa against 34.7 and 44.6 MPa, for FL9 and CL6 respectively). In the case of quartz, the addition of CQ, compared to FQ leads to better performance from 2 days to 28 days (CQ6 values ranging, up to 28 days, from 17.8 to 40.3 MPa against 13.3-34.2 for FQ6). However, at 56 days, the incorporation of FQ surpasses these results due to a greater increase of the compressive strength between 28 and 56 days compared to CQ (45.1 for CQ6 and 47.1 MPa for FQ6). Overall, the highest values are obtained with FL addition and a maximum of 48.5 MPa at 56 days was reached for FL9. An optimal volume percentage of 6 is found for the other fillers tested. The absence of improvement in compressive strength for all filler-containing samples compared to the reference at 2 days is in accordance with the calorimetry results. Furthermore, the positive effect of fillers, observed at a later age instead, could be due to the lower reaction rate of C<sub>2</sub>S [48]. The better impact of FL compared to FQ, on the performance of the binder starting at 28 days, is in accordance with the literature about OPC systems [28].

# 5.2.1. Phase quantification

The phases are identified by performing XRD.  $C_2S$ , brownmillerite, and wuestite are detected. Magnetite, considered inert is also still present [12,18]. Examples of the patterns obtained for the reference sample, FL6, and FQ6 at different ages can be found in the Appendix A, in Figures A1, A2, and A3, respectively. Quartz is detected in the F/CQ samples and calcite is identified in the F/CL samples, even though due to slight carbonation of the samples small amounts of calcite are detected in F/CQ samples as well.

The phase amounts in all the samples at 7, 28, and 56 days are quantified and the results normalized, by removing the filler content and the chemically bound water amount, as:

$$X_N = \frac{X_i * 10000}{100 - X_f} * \frac{1}{100 - X_{cbw}}$$
 (2)

With Xi, the initial fraction,  $X_f$  the percentage of filler in the mix, and  $X_{chw}$ , the water loss in the range of temperature 40–540°C.

This approach ensures a direct comparison with the unreacted BOF slag phase quantification. The evolution of the reactive slag phases and the hydration products, in the samples containing fine fillers, are presented in Figs. 4 and 5, respectively. The normalized and the original quantification values of all the samples are given in the Appendix A, in Tables [A2; A9]. A relative error of 6.8 % can be determined for magnetite based on the variations in the QXRD results. Magnetite (Fe<sub>3</sub>O<sub>4</sub>) can be considered inert based on previous literature about BOF slag hydration [12,14,18,19]. The same error was also applied to the other phases.

The unreacted BOF slag contains  $C_2S$  ( $Ca_2SiO_4$ ) (40 wt%), brown-millerite ( $Ca_2(Al, Fe)_2O_5$ ) (16.7 wt%), wuestite (Fe(Mg)O/Mg(Fe)O) (18.4 wt%), a small amount of magnetite (6.3 wt%) and a very low

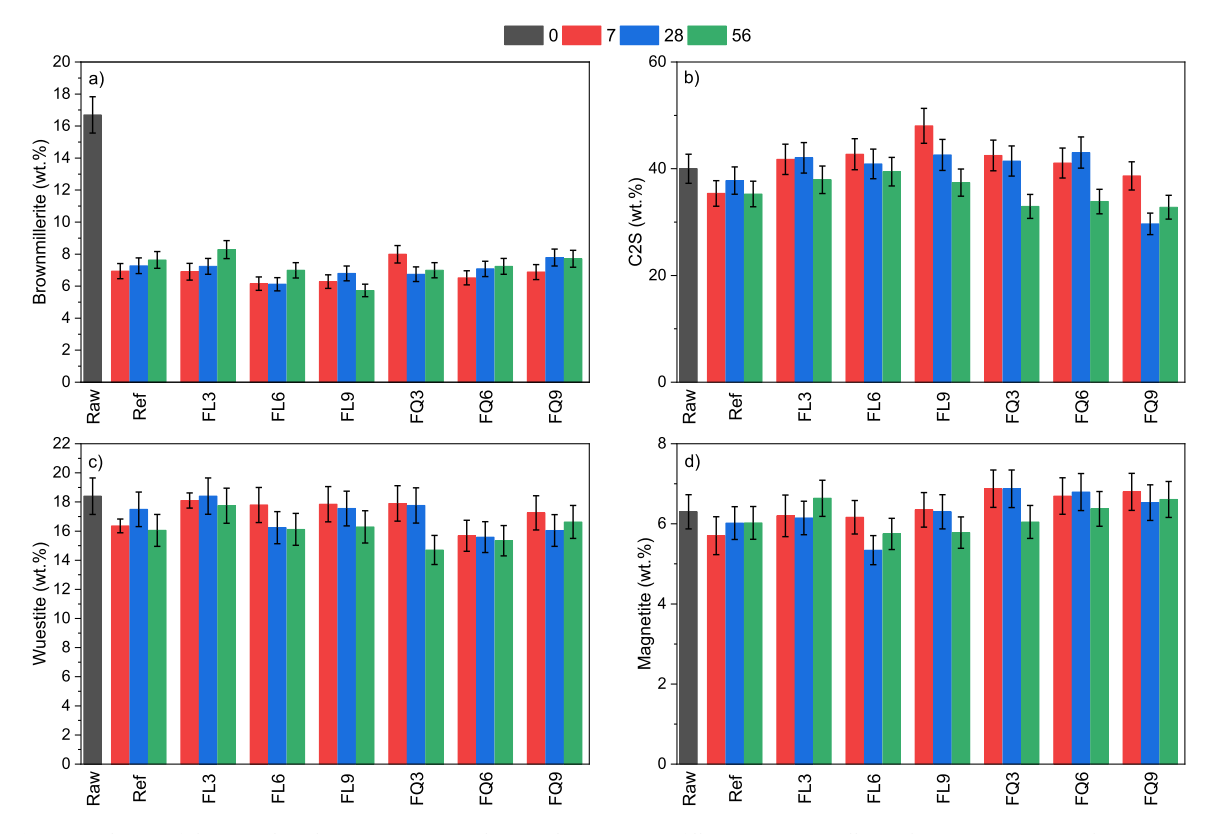


Fig. 4. Evolution of the BOF slag phases over time in the samples containing fillers, (a) Brownmillerite; b) C2S; c) Wuestite; d) Magnetite).

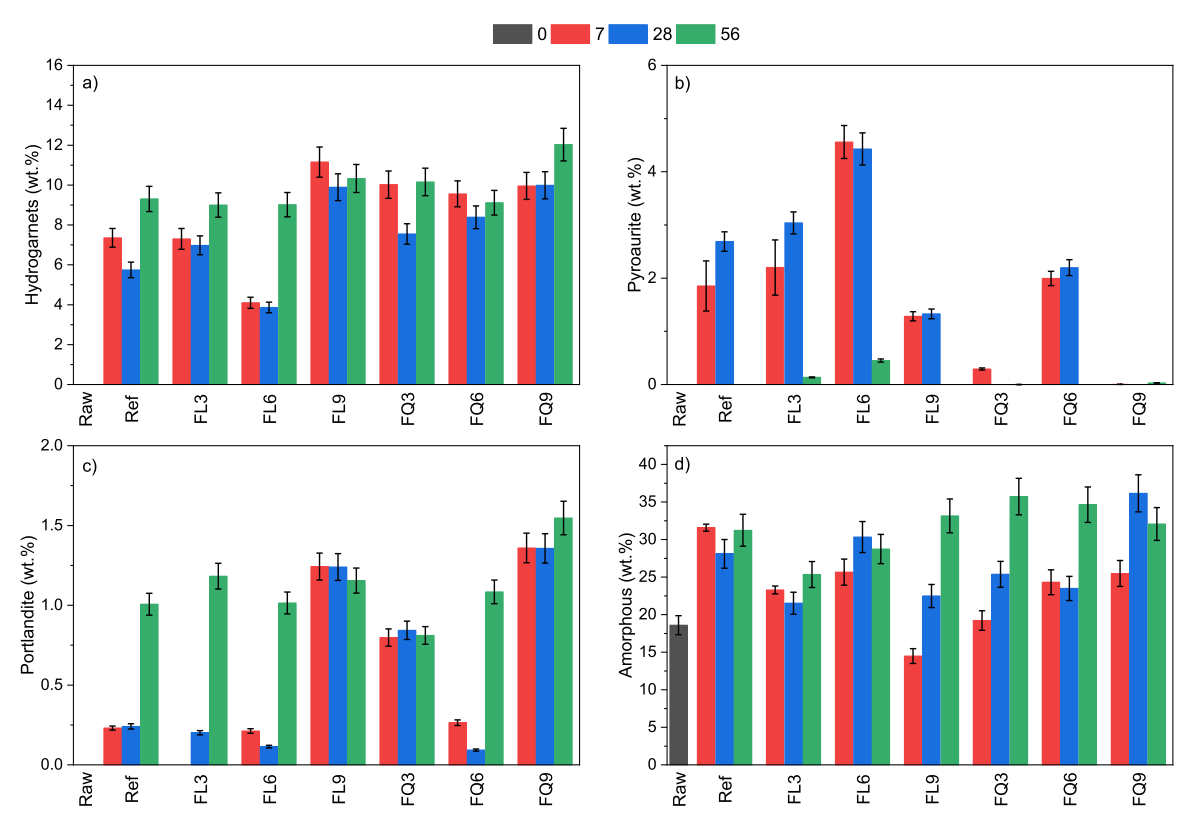


Fig. 5. Evolution of the formed hydration products and amorphous content over time in the samples containing fillers, (a) Hydrogarnets; b) Pyroaurite; c) Portlandite; d) Amorphous).

amount of free lime (CaO) of around 0.4 wt%. An amorphous part, representing about 18 wt% of the BOF slag was also measured. As BOF slag is known to be 100 % crystalline after production [49], it is important to note that the initial amorphous content in the raw BOF slag might be due to the loss of crystallinity of certain phases during milling Santos et al. [12] reported that the amorphous content in unhydrated BOF slag increases with milling time, accompanied by a reduction in C<sub>2</sub>S content. The X-Ray amorphization of such phases by milling has also been discussed in the literature [50,51], highlighting a better resistance of C<sub>4</sub>AF during dry grinding, compared to the one of C<sub>3</sub>S and C<sub>2</sub>S. This supports the findings of Santos et. al suggesting that X-ray amorphized C<sub>2</sub>S might be present in milled BOF slag, leading to a reduction of the quantified amorphous amount while reacting. [12,19].

In the reference sample, it is observed that around 60 % of the brownmillerite reacts within the first 7 days due to the presence of tripotassium citrate as demonstrated in [18,19]. C<sub>2</sub>S and wuestite react very slowly with about 12 % and 11 % being consumed at 7 days, respectively. Lime (CaO) is quantified at around 0.5 wt% in our samples, similarly to the raw material. The crystalline hydration products identified are mainly Fe-containing hydrogarnets (Ca<sub>3</sub>(Al, Fe)<sub>2</sub>(OH)<sub>12</sub>) [39], along with a small amount of portlandite (Ca (OH)2), and calcium carbonates (CaCO<sub>3</sub>). A minor presence of pyroaurite (Mg<sub>6</sub>Fe<sub>2</sub> CO<sub>3</sub>(OH)<sub>16</sub>.4H<sub>2</sub>O) is also suggested, based on literature [12,17,18], and supported by a peak observed at 13°20 in the XRD patterns [40], although this signal is very close to the detection limit. Regarding the amorphous content, an increase of about 70 % is observed, attributed to the formation of non-crystalline hydration products, mainly C-S-H. Between 7 and 56 days the different crystalline phases, as well as the amorphous content, stay stable. Hydrogarnet content increases after 28 days of hydration, while the pyroaurite tends to disappear. Santos et al. reported a decrease in pyroaurite content in hydrated BOF slag pastes, falling below the XRD detection limit over time. The reduction observed in the citrate-activated samples is consistent with these findings, suggesting that the small amount detected at early age is either unstable or becomes X-ray amorphous over time [12].

In the samples containing fillers, quartz is detected in the F/CQ samples and calcite is identified in the F/CL samples, even though due to slight carbonation of the samples small amounts of calcite are detected in F/CQ samples as well. Among the primary phases, brownmillerite and wuestite are also reacting. Therefore, the presence of filler does not prevent the effect of citrate on the reactivity of these two phases [18]. However, under the present conditions, the fillers do not appear to significantly promote the hydration of these phases. This contrasts with the behaviour observed in OPC systems, where limestone is often reported to accelerate the dissolution of clinker phases. The C<sub>2</sub>S is slightly reducing over time compared to the reference for which the C2S content stays stable after 7 days. The same 3 types of crystalline hydration products are found. A small amount of portlandite is quantified, which shows a slightly increased amount in the samples containing 9 vol% fillers. Hydrogarnets are still the main hydration product formed. The hydrogarnet content after 7 days is between 4.1 and 11.2 wt%, with CL3/FL3CL6, CL6/FL6, CQ6, and the reference having the lowest contents between 4.1 and 7.6 wt%, while all the other samples are between 9 and 11.2 wt%. The amount remains largely unchanged at 28 days, although some samples show a slight decrease. At 56 days the amount of hydrogarnet increases and is between 8.6 and 12.9 wt%, with the largest increase occurring for the samples with the lowest content at 28 days. There is no clear difference between limestone and quartz-containing samples. After 7 days of hydration, the portlandite content is highest in samples CL9/FL9, CQ3/FQ3, CQ9/FQ9 with values between 0.8 and 1.4 wt%. All other samples show much lower content of 0-0.3 wt%. Similar to hydrogarnet, this remains largely unchanged at 28 days and begins to increase in the samples with a lower initial portlandite content at 7 days, especially in the reference and CL3/FL3. At 56 days the values are between 0.8 and 1.5 wt% in all the samples except CQ3 and CQ6 which contain 0 wt% of portlandite. Only minimal differences were

observed between the fine and the coarse filler. However, when comparing limestone and quartz in general distinct trends were observed, particularly concerning the C2S and amorphous content. Although the consumption of C<sub>2</sub>S at 7 and 28 days appears comparable, at 56 days around 17 wt% of C2S is being consumed when quartz is incorporated against only 4 wt% of the starting C2S for limestone addition. The amorphous content, which is assumed to include mostly C-S-H gel, is generally smaller in the samples including fillers, in contrast with the reference. This amorphous content stays stable over time for most of the samples except for FL9 and FQ3. Notably, FL9 exhibits a significant reduction in amorphous content up to 7 days of hydration, decreasing from 18.6 wt% in the unreacted material to 14.5 wt% in FL9 at 7 days (-22 %). This observation may suggest a negative impact of these fillers on C-S-H formation, even though the C<sub>2</sub>S consumption stays either uninfluenced or promoted in the case of quartz. However, it should be noted that the initial amorphous content in the raw BOF slag studied is attributed to the possible mechanical amorphization of the crystalline C<sub>2</sub>S as previously discussed [12,18,50,51]. Based on this, it may be hypothesised that the amorphous content in all the sample includes not only the hydration products but also X-Ray amorphized phases such as C<sub>2</sub>S. This might explain why the amorphous content is reducing for some samples, alongside a reduction of the crystalline phases and no increase of the crystalline hydration products. Essentially part of the amorphous content (the C2S) is reacting, while also forming amorphous hydration products making the overall amorphous lower or remain stable in some samples. However, after 7 days, the amorphous part in FL9 increases significantly to reach 33.1 wt%, revealing the formation of more amorphous hydration product most likely C-S-H gel.

# 5.3. Thermogravimetry analysis

Thermogravimetric analyses were performed on all pastes hydrated for 7, 28, and 56 days. The TG and DTG curves of the reference are presented in Fig. 6. The differential mass loss in the reference samples is attributed to the decomposition of C-S-H, hydrogarnets, portlandite, and carbonates. The portlandite and the carbonates decompositions are reported to occur around 450°C and from 600 to 800°C, respectively. For pyroaurite, C-S-H, and hydrogarnets, the decomposition is reported to take place within a wide range of 40-400 °C due to their variable composition. Nevertheless, according to the literature, the distinguishable peaks observed between 100 and 200°C and between 200 and 400°C can be attributed to C-S-H and pyroaurite dehydration and hydrogarnets decomposition, respectively [52–54]. The mass loss increases over time with more water bound in C-S-H, slightly more hydrogarnets and portlandite are formed and more carbonates are present as well. This is in accordance with what was previously reported about citrate-activated BOF slag [18,19].

Figs. 7 and 8 report the results of the samples incorporating fine fillers and coarse fillers, respectively. The mass loss values per temperature range, reported in the Appendix B in Table B1, B2, B3, and B4, are normalized by the weight of BOF slag with the following equation,

$$X_N = \frac{Xi * 100}{100 - X_f} \tag{3}$$

With,  $X_N$  is the normalized mass loss,  $X_i$ , the initial mass loss, and  $X_f$  the percentage of filler.

The samples containing the fillers all show a similar trend with increasing age. No clear trend in relation to the filler size and amount can be found, however, differences between quartz and limestone are observed. For the samples hydrated for 7 days, the effect of the filler is minimal. For the reference sample, the water loss in the range 40–200°C equals 3.37 wt% and 2.39 wt% in the range 200–400°C. For all the other samples at this age, the water loss in the range 40–200°C varies between 2.86 and 4.31 wt% and between 2.12 and 3.12 wt% in the range 200–400°C. The portlandite formation is slightly influenced by the incorporation of fillers but the overall amount is very low, the measured

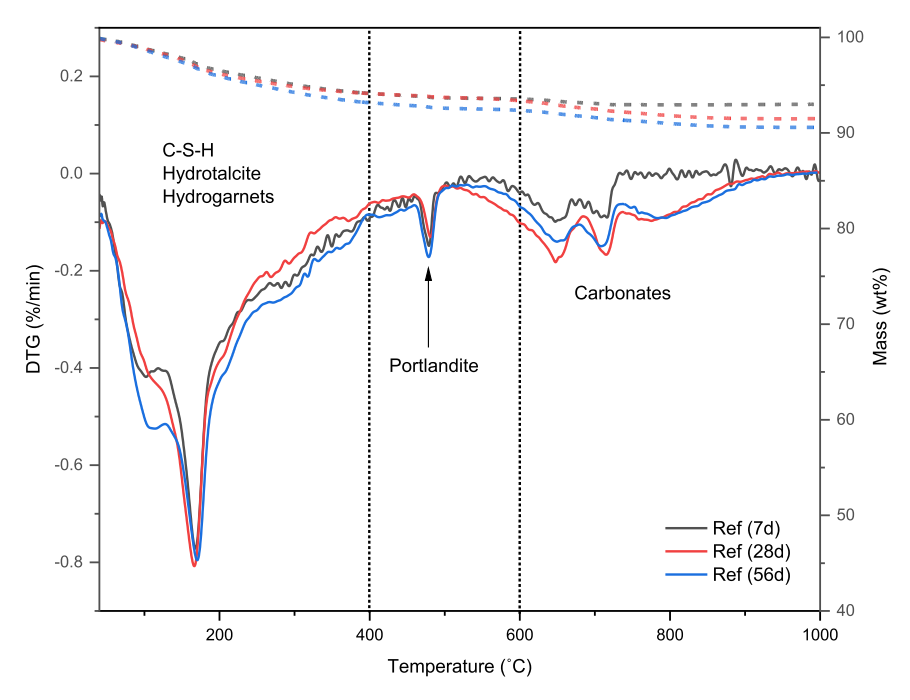


Fig. 6. TG and DTG curves of BOF slag pastes without filler hydrated for 7, 28, and 56 days.

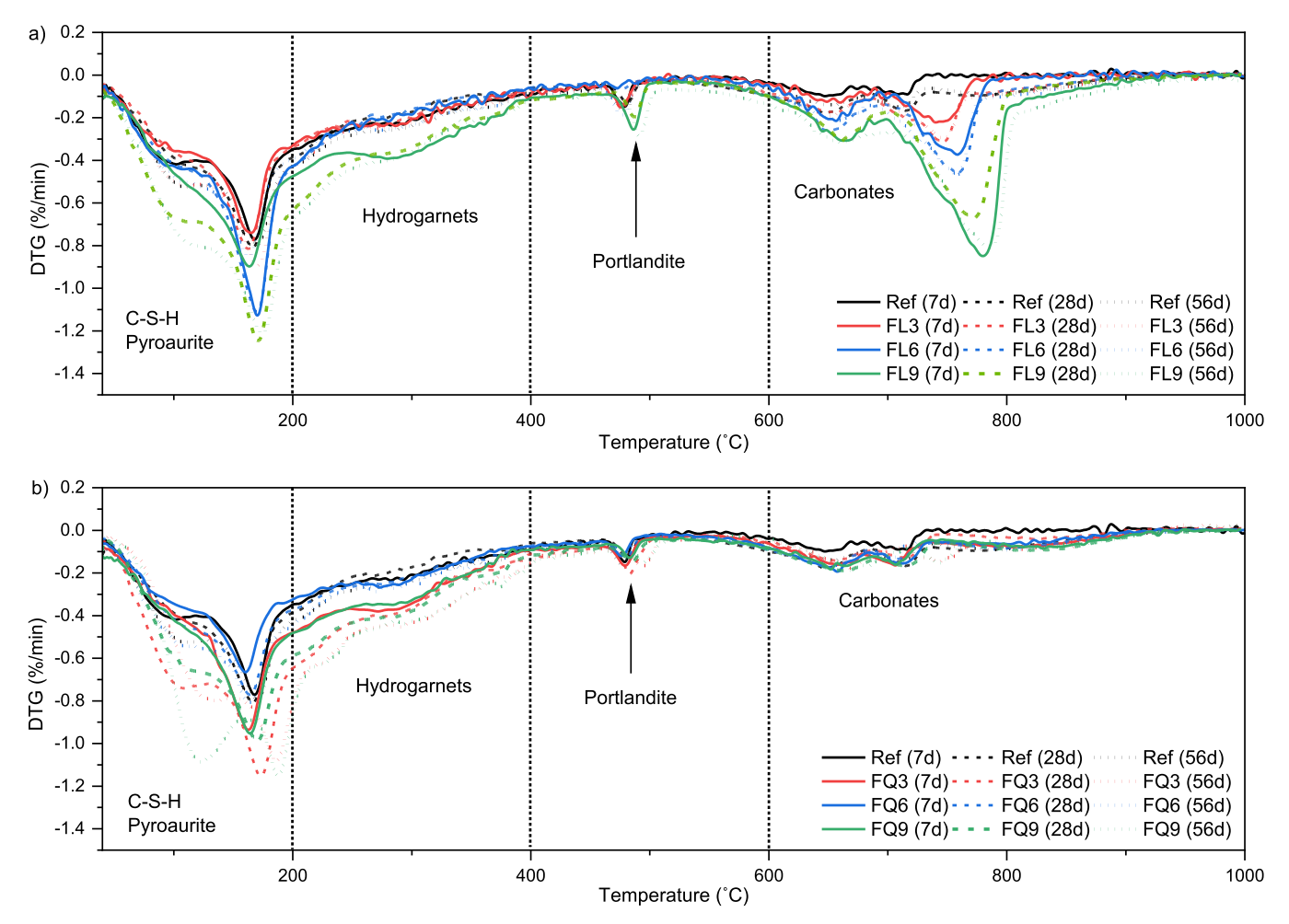


Fig. 7. DTG curves of the BOF slag pastes containing fine fillers hydrated for 7, 28, and 56 days, (a) Fine limestone (FL); b) Fine quartz (FQ)).

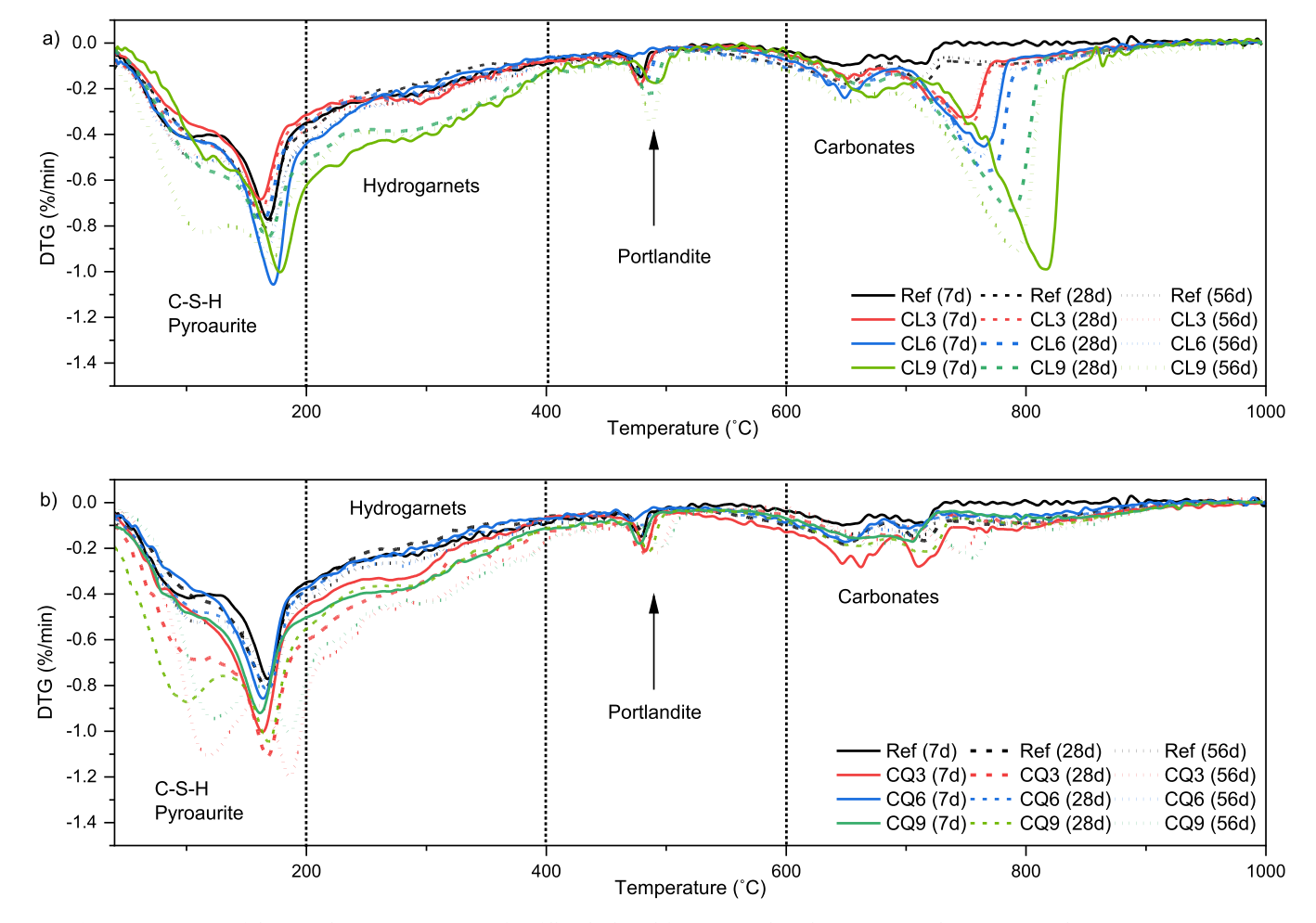


Fig. 8. DTG curves of the BOF slag pastes containing fine fillers hydrated for 7, 28, and 56 days, (a) Coarse limestone (CL); b) Coarse quartz (CQ)).

water loss varies from 0.07 to 0.3 wt%. This is in accordance with the literature about portlandite formation from  $C_2S$  hydration [48]. At all ages, the amount of carbonates is not influenced by the presence of fillers. The increased mass losses in the range 600–800°C for the limestone-containing samples are due to the decarbonation of the limestone itself. That is why it is proportionally increasing with the percentage of limestone added.

Starting at 28 days, the differences between limestone and quartz-containing samples are clearer. In the case of limestone, more water was bound in the C-S-H region of the samples containing 9 vol% of limestone, compared to the reference, FL3, and FL6 samples. In the case of quartz addition, both C-S-H and hydrogarnets formation are

**Table 5**Total porosity of samples hydrated for 28 and 56 days, assessed with MIP.

	Total porosity at 28 days	Total porosity at 56 days
	%	%
Ref	17.5	16.9
FL3	17.4	17.0
FL6	14.6	13.3
FL9	14.1	3.7
CL3	17.1	15.2
CL6	12.3	13.9
CL9	16.1	14.7
FQ3	15.6	18.0
FQ6	17.6	17.1
FQ9	14.1	17.1
CQ3	14.7	15.4
CQ6	14.1	17.9
CQ9	16.4	8.7

positively influenced by 3 and 9 vol% of quartz. However, for a dosage of 6 vol%, no difference with the reference mix curve is observed. Moreover, within the C-S-H dehydration range, the FL9/CL9 DTG curve exhibits a prominent peak at 180 °C, similar to the other limestone-containing samples, along with a small bump around 120 °C. Conversely, the FQ9/CQ9 DTG curve shows two distinct peaks: one at 120°C and another at 190°C. This suggests a shift of the primary peak due to the decomposition of certain hydration products at 120°C.

# 5.4. Porosity and pore structure

The total porosity of the different samples is reported in Table 5. At 28 days the total porosity of the ref is 17.5 %. The incorporation of fillers slightly reduces the porosity at 28 days, but the size and the nature of the fillers do not lead to great differences with values ranging from 17.6 % to 12.3 %. At 56 days of hydration, the porosity varies from 18 % to 3.7 %. The highest porosity is observed in the quartz samples, especially the FQ samples (17.1–18 %). Limestone samples have reduced porosity. For CL addition there is little influence on the dosage. The porosity only slightly varies from 13.9 % to 15.2 % depending on the dosage. However, for FL there is a clear decrease in total porosity with the increased dosage, ranging from 17 % to 3.7 %. For all the other samples no trend regarding the dosage is found.

The pore size distribution of the BOF slag pastes hydrated at 28 and 56 days are reported in Figs. 9 and 10, respectively. Three categories of pores are distinguished in the literature [55–57]. Gel pores are attributed to the internal porosity of the gel and range from 5 nm up to 10 nm. The small capillary pores, from 10 nm to 50 nm, refer to the voids between the hydration products. The large capillary pores from 50 to 10,

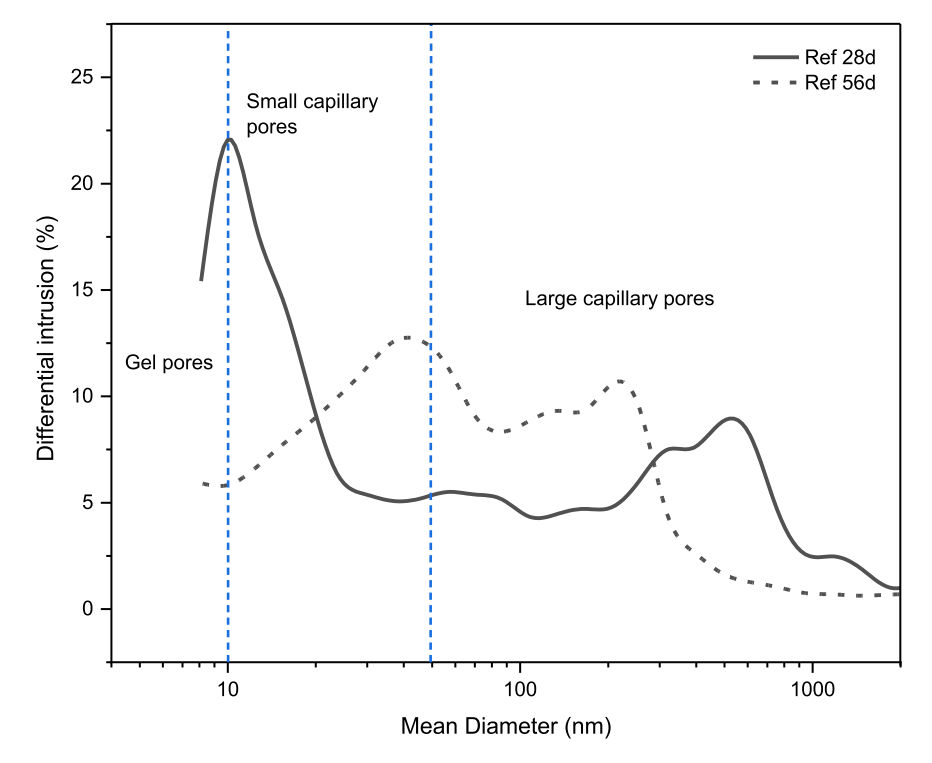


Fig. 9. Pore distribution measured with MIP of hardened BOF slag pastes at 28 and 56 days.

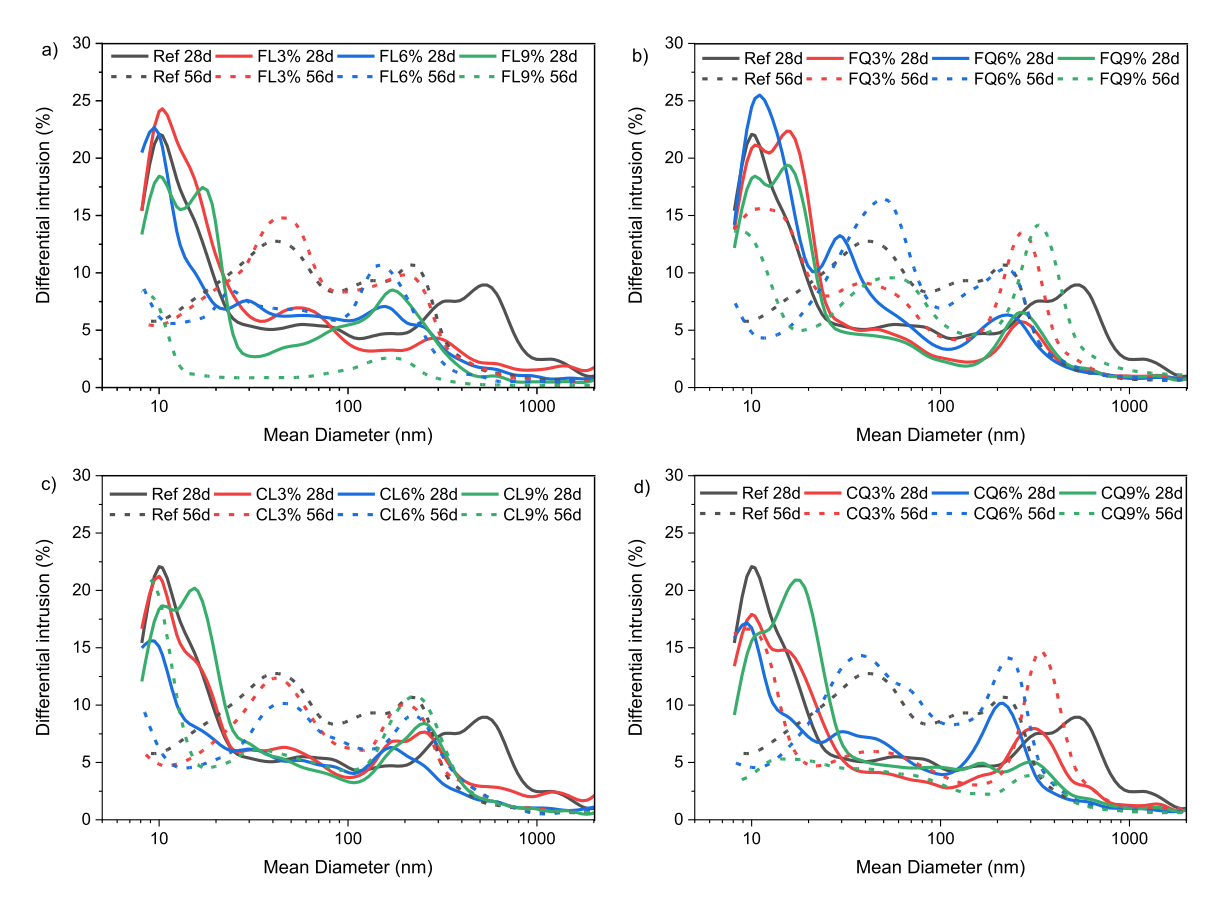


Fig. 10. Pore distribution measured with MIP of hardened BOF slag pastes containing fillers at 28 and 56 days, (a) Fine limestone samples; b) Fine quartz samples; c) Coarse limestone samples; d) Coarse quartz samples).

000 nm, correspond to the voids, initially filled with water, left out of hydration products. At 28 days, a reduction of the large capillary-pore content in the mixes containing fillers is observed as the peak of the reference in the range 200–1000 nm shifts towards the smaller size pores. It can be attributed to an improvement of the particle packing with the addition of fillers or to a higher content of hydration products.

At a later age, it is first observed that the overall size of the large capillary pores is reduced, with a peak observed at 28 days in the range 200 – 1000 that is at 56 days observed in the range 100–400 nm for the reference sample. In the case of limestone filler, the amount of large capillary pores does not change with the dosage; however, some differences are observed with the mixes containing quartz. 3 and 9 vol% of FQ addition increases the number of large capillary pores, while 6 % increases the number of small capillary pores. This could be due to a higher amount of crystalline hydration products and, subsequently, their internal porosity. This also results in an increased total porosity of some samples. This Over time, the amount of gel pores measured with MIP decreases, probably due to a reduction of their size that makes them undetectable with MIP [56,58]. Nevertheless, the total porosity reduction in FL9 and CQ9 cannot be completely attributed to a possible shift toward the smaller size. It is also clear that the capillary pores are significantly reduced in those samples. Although differences in pore size distribution and total porosity were observed across the samples, all values remain relatively low. The narrow range of porosity, combined with the limitations of MIP (ink-bottle effect and detection thresholds) [52], likely contributes to the weak or inconsistent correlation with compressive strength. As shown in the correlation section (Figs. 13–15), strength evolution does not consistently follow changes in porosity or type of pores. This suggests that other factors, such as the amount and type of hydration products, play a more dominant role in strength development than porosity alone.

### 6. Correlation and discussion

The use of filler in binders is reported as enhancing the clinker phases dissolution, the formation of binding hydration products, and therefore the performances of the binder. This is due to three mechanisms: (1) the

increased shearing between the reactive grain surface and the fillers, and a reduced porosity due to better particle packing; (2) the dilution of the material; (3) the presence of extra nucleation sites. In OPC binders the beneficial effect of a small amount of filler was demonstrated to be due to an enhanced dissolution of  $C_3S$  and the rapid formation of  $C_3S$ -H nuclei on the surface of the filler grains preferentially to the cement grains. Therefore, by decreasing the PSD and increasing the specific surface area the fillers become more effective.

In the present study, filler addition was investigated for the first time on BOF slag and showed good improvement in the binder strength. The positive effect of filler addition becomes evident at 56 days of curing, with both quartz and limestone contributing to a  $12–55\,\%$  increase in the compressive strength of the BOF slag binder, respectively. An optimal 6 % volume replacement was found for all fillers except for fine limestone, which shows better influence with a dosage of 9 %. These improvements might be explained by the accelerated dissolution of  $C_2S$ , the reduction of the total porosity of the samples, or an enhanced formation of hydration products, contributing to the strength development. However, there is a limited correlation between the properties and the filler type and quantities.

Therefore, an impact factor statistical model (two-way ANOVA) was performed to assess the impact of the parameters age of the sample, filler nature, filler size, and filler dosage on the compressive strength, the mass loss (TGA), the hydration product content (XRD) and the porosity, (gel porosity, small capillary porosity and total porosity). Six different combinations of factors were applied. The p-values (level of significance) obtained are summarized in the Appendix C. This analysis revealed a significant influence of all parameters on the compressive strength, with p 0.01, p 0.01, and p 4.94E-4 for the filler nature, filler size, and dosage, respectively. However, the p-values for age were always the lowest (around 1E-10). These results are in accordance with the Fig. 11, which shows the influence of the hydration product amount on the compressive strength.

The amount of bound water as determined with TG is only significantly influenced by age and to a lesser extent by dosage of the filler (p-1E-4 and p-1E-3), while the amount of hydration products (crystalline + amorphous content) detected with XRD only has a limited correlation

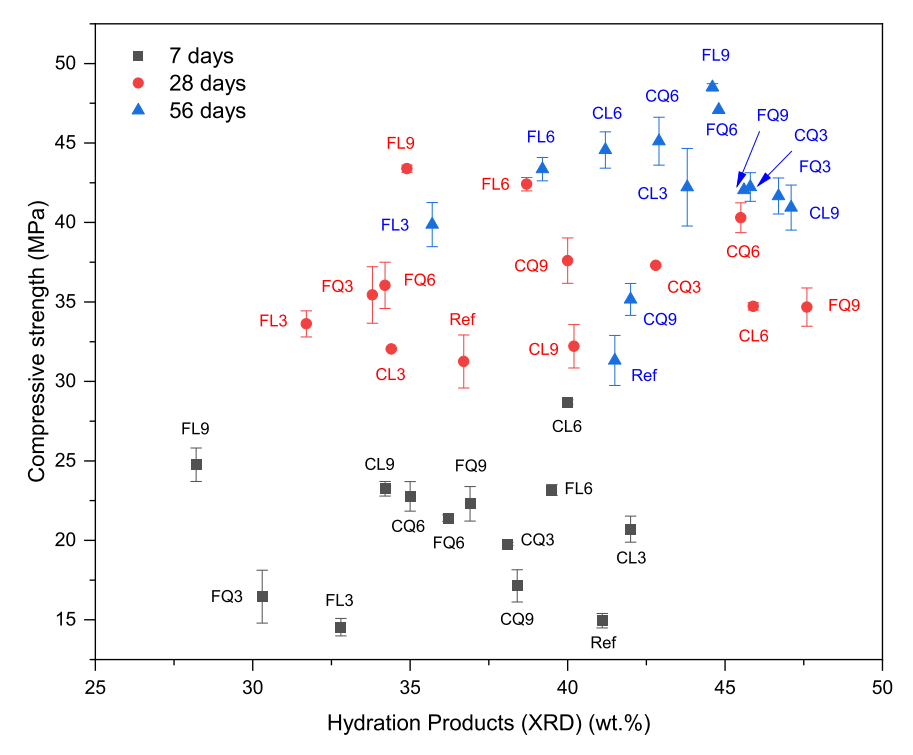


Fig. 11. Compressive strength vs amount of hydration products determined with Q-XRD at 7, 28, and 56 days.

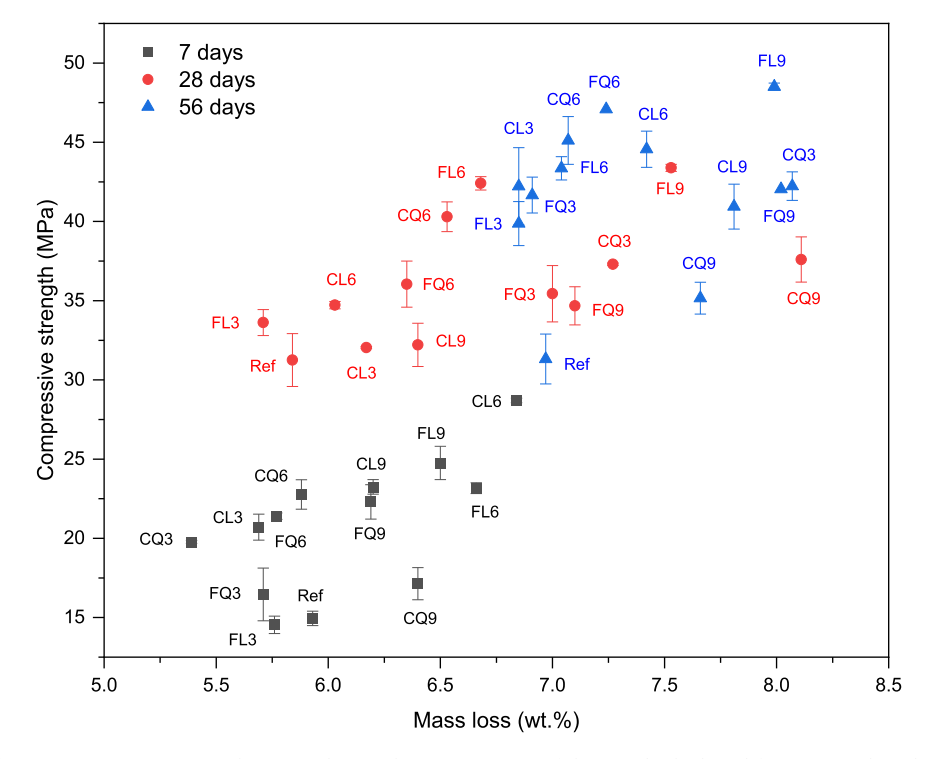


Fig. 12. Compressive strength vs mass loss in the range 40–540 of the samples hydrated for 7, 28, and 56 days.

with age (p 0.05). This limited correlation is illustrated in Fig. 11, where no clear trend is observed between the hydration product content and the compressive strength over time. One hypothesis might be the complexity of the amorphous phase which likely includes both amorphous hydration products (mostly C-S-H gel) and X-Ray amorphized reactive phase, likely  $C_2S$  [12,50,51]. Consequently, a lower amorphous content will not necessarily lead to a lower strength in the samples, as it might indicate the consumption of the amorphous part in the unreacted

slag after milling and not necessarily a low amount of C-S-H. TGA therefore gives clearer insights into the formation of hydration products, without being influenced by the potential presence of X-Ray amorphized  $C_2S$ . As shown in Fig. 12, the mass loss in the temperature range 40 – 540°C correlates more significantly with the compressive strength over time, supporting the statistical analysis findings. The increase in chemically bound water follows a progressive strength gain over time. This might be attributed to the formation of more hydration products or

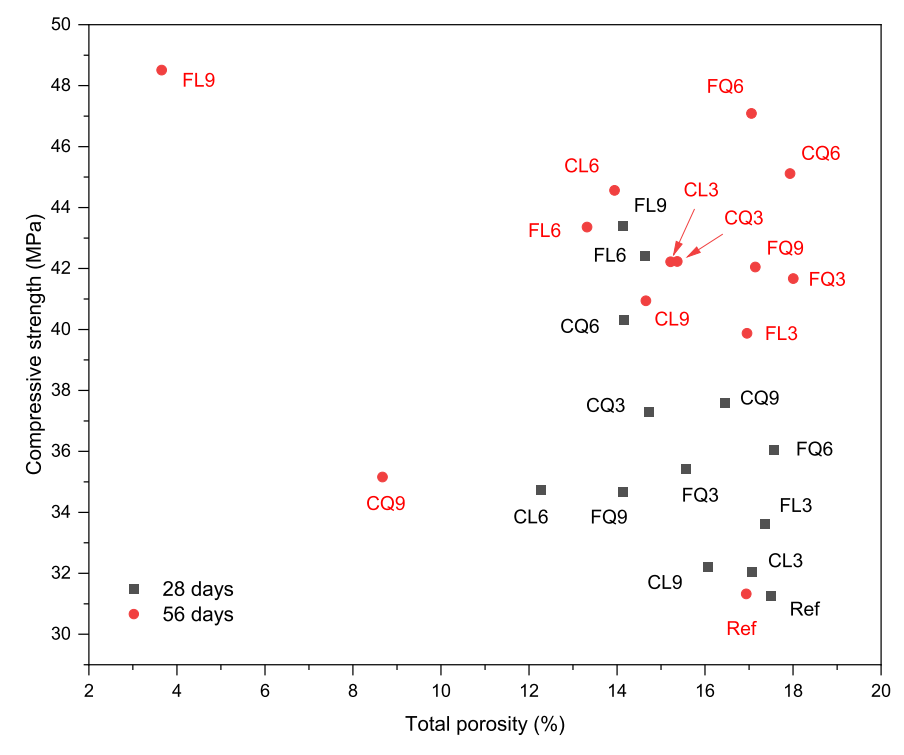


Fig. 13. Compressive strength vs total porosity of the samples containing fine limestone filler measured with MIP at 28 and 56 days.

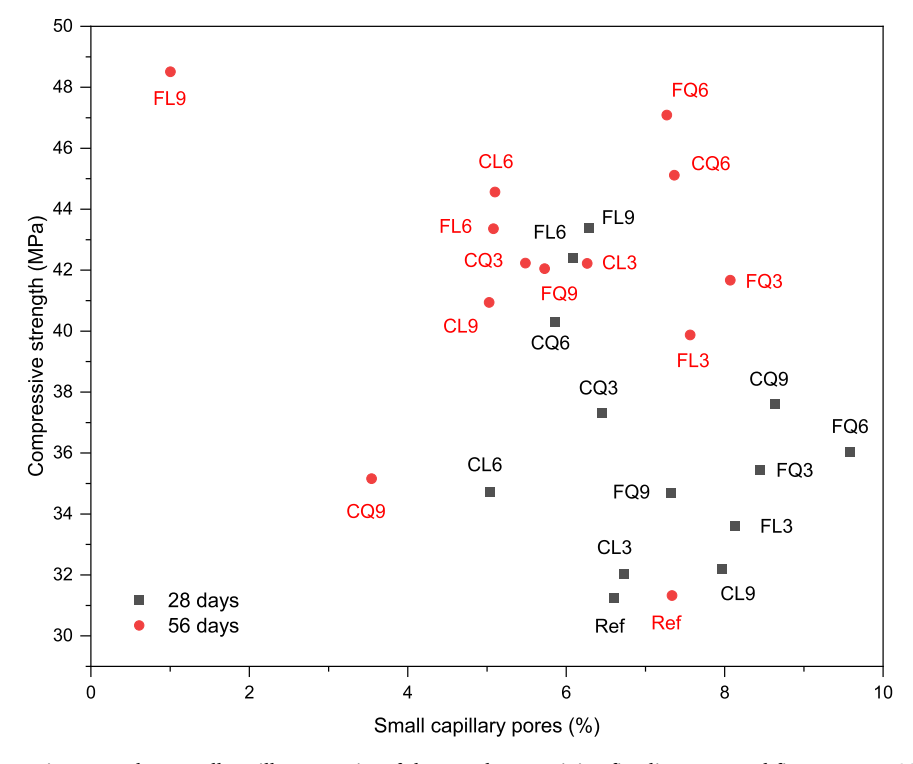


Fig. 14. Compressive strength vs small capillary porosity of the samples containing fine limestone and fine quartz at 28 and 56 days.

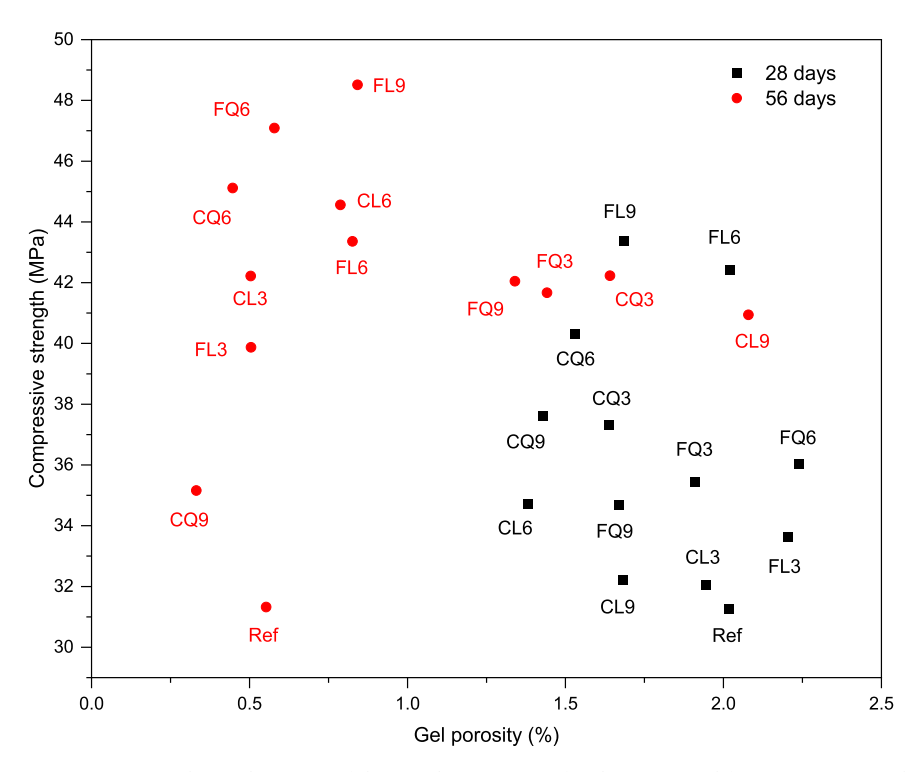


Fig. 15. Compressive strength vs gel porosity of the samples containing fine limestone and fine quartz at 28 and 56 days.

phase transformations in the (amorphous) hydration products. A higher amount, or a reorganization or densification, of the hydration products – particularly C-S-H - leads to a better compressive strength of the binder.

The increase in strength, and subsequently a possible higher amount of amorphous hydration products might be reflected in the porosity of the samples. The total porosity is known to have a high impact on the compressive strength of OPC binders [59–61]. Figs. 13–15 show the

evolution of the compressive strength with the total porosity, the capillary porosity, and the gel porosity, respectively. Considering the entire set of samples no trend is observed between the strength and the total and the capillary porosity, oppositely to what was expected based on the literature. The statistical model showed, indeed no direct influence of the different parameters on the total porosity and the capillary porosity while it was influencing the strength. These observations might

be explained by (1) very similar porosity values among the different samples; (2) similar amount of crystalline hydration products; and (3) the lack of influence of the filler on the particle packing due to their PSD comparable with the one of BOF slag.

Nevertheless, the gel porosity shows a different behaviour. Fig. 15 clearly reveals a reduction of the gel porosity in the samples, between 28 and 56 days. The two-way ANOVA gives indeed p-values around 1E-4 for the influence of the factor age on the gel porosity. The reduced gel porosity between 28 and 56 days might be due to a reduction of their size, making them undetectable with MIP. A size reduction may be attributed to a refinement of the porosity in the hydration products. Regarding the influence of the filler on the gel porosity, the combination of the parameters filler nature/filler dosage and the combination filler nature/filler size result in p-values very close to the statistical limit of 0.05, (0.11, 0.10, and 0.07). This may also indicate an influence of the type of filler on the hydration product amount and structure.

To confirm the influence of microstructural parameters on compressive strength, a multiple linear regression analysis was performed with the R software. The resulting model (Appendix C) confirmed that mass loss was the only statistically significant predictor (p-value =0.049), with a positive coefficient indicating that increase in chemical bound water leads to an increase in strength. All other variables, including hydration product content and porosity types, did not reach statistical significance within the combined model. The overall efficiency of the model is moderate, with an  $R^2$  of 0.42. In comparison, a simplified model including only mass loss as a predictor yielded a higher  $R^2$  of 0.57 and a stronger coefficient (p-value <0.001), confirming that the mass loss alone is a better indicator of strength development than the combination of all other variables.

Generally, literature reports a superior effect of limestone due to its ability to act as a calcium ion sink and a favourable substrate for C-S-H nucleation [29,42,62]. In line with this, limestone-containing samples performed slightly better than those with quartz, although quartz also contributed positively to strength. Despite the relatively low statistical impact of filler type, differences in hydration behaviour and microstructure were observed between the two.

Fine limestone enhanced the hydration product formation and reduced the porosity, particularly in FL9, which achieved the highest compressive strength and the lowest porosity. These observations could corroborate the TG and the XRD results by suggesting a higher amount of hydration products that create a denser structure. However, no clear influence on the  $\rm C_2S$  reactivity was observed. While XRD analysis did not reveal a clear consumption of crystalline  $\rm C_2S$  over time, TG analysis showed an increased amount of C-S-H gel with the addition of fillers. This suggests again the possible involvement in the reaction, of the amorphized phases, formed during the milling of BOF slag.

Fine quartz also improved strength, with the best result at 6 % replacement. However, the influence of the microstructure on the compressive strength follows the opposite direction compared to limestone filler. Although FQ6 and CQ6 samples showed lower hydration product amounts than FQ3/FQ9 and CQ3/CQ9 in TG and XRD, they achieved the best strength among the quartz-containing samples. This suggests that hydrate assemblage is different when quartz is added in comparison with limestone. The higher mass loss values for FQ3/CQ3 and FQ9/CQ9 compared to FQ6/CQ6, are due to the appearance at 28 days of a second peak very pronounced in the range of 40-150 °C. Although pyroaurite may decompose in this temperature range, a notable increase in its content appears unlikely, as it would not align with the XRD results. Another explanation could be that the peak is due to the water loss of a "second" C-S-H gel with a lower Ca/Si ratio. As shown by Scrivener et al. [52,63], the temperature of C-S-H dehydration reduces with the reduction of the Ca/Si ratio. Moreover, it has been reported that the formation of a C-S-H gel with a lower Ca/Si ratio can lead to lower performances [64]. Regarding the porosity and pore structure, no good correlation with the compressive strength can be found. A higher amount of capillary pores is found in FQ6 which also

exhibits the highest strength, contradicting the literature [55–58]. However, it has been observed for FQ6 that the large capillary pore size is reduced at 56 days compared to FQ3 and FQ9, for which the capillary porosity size stays the same between 28 and 56 days. This could suggest that the hydration products formed in FQ6 are densifying over time while new porous hydration products are formed in FQ3 and FQ9.

Overall, the data show that neither total porosity nor pore type shows a consistent relationship with strength in this system. Instead, strength development appears to be more strongly influenced by the extent and nature of hydration, particularly as captured by chemically bound water measured via TGA. This reinforces the conclusion that, in citrate-activated BOF slag binders, strength is governed by complex chemical and structural factors rather than simple porosity metrics.

## 7. Conclusion

This study investigated the influence of small additions of limestone and quartz fillers on the performance and microstructure of tripotassium citrate-activated BOF slag. The results demonstrates that filler incorporation positively impacts the compressive strength of the binder and modifies the hydrate assemblage and porosity of the paste. These findings provide valuable insights into the role of fillers in BOF slag-based systems. The key outcomes are summarized as follows:

- Small additions of both limestone and quartz fillers significantly improve compressive strength between 7 and 56 days.
- The presence of fillers does not interfere with the activation effect of tri-potassium citrate.
- Fine fillers generally lead to slightly better mechanical performance compared to coarse ones.
- An optimal dosage of 6 vol% was identified for coarse limestone, coarse quartz, and fine quartz. Fine limestone at 9 vol% leads to the highest strength, approximately 55 % higher than the reference.
- Both fillers promote the formation of hydration products, particularly C–S–H gel, as shown by TGA.
- A slight reduction in porosity is observed in the presence of fillers, likely due to increased hydration product formation.

However, the observed strength gains do not directly correlate with the microstructural data, primarily due to limitations in the characterization techniques. In particular, it remains difficult to assess potential improvements in  $C_2S$  reactivity, given the presence of amorphized  $C_2S$  at early ages, which cannot be tracked by XRD. Similarly, the amorphous nature of  $C_2S$ —H and the potentially low crystallinity of phases such as hydrogarnet and pyroaurite make it challenging to detect clear differences between samples. In addition, variations in the structure and composition of the hydration products may influence the material properties without being fully captured by TGA. Although changes in porosity and pore structure were observed, they did not consistently correlate with strength development. In contrast, chemically bound water measured by TGA showed a stronger association with mechanical performance.

To address these limitations and better understand the mechanisms underlying the effects of limestone and quartz fillers, further investigation is recommended. Future work may focus on higher filler dosages and more advanced characterization of the amorphous phase composition in BOF slag systems. In addition, although dimensional stability was not a concern in this study due to the low free lime content of the BOF slag used, expansion remains a potential issue in slags containing higher amounts of free CaO. It is therefore recommended that future studies on citrate-activated BOF slag systems assess volume stability, particularly when working with slags known to exhibit significant expansion risks.

# CRediT authorship contribution statement

K. Schollbach: Writing - review & editing, Visualization,

Supervision, Methodology, Conceptualization. T. Wattez: Writing – review & editing, Visualization, Supervision, Resources, Methodology. S. Van der Laan: Writing – review & editing, Supervision, Resources. H. J.H. Brouwers: Writing – review & editing, Supervision, Resources, Project administration, Funding acquisition. S. Yvars: Writing – review & editing, Writing – original draft, Visualization, Methodology, Investigation, Formal analysis, Conceptualization.

### **Declaration of Competing Interest**

The authors declare that they have no known competing financial interests or personal relationships that could have appeared to influence the work reported in this paper.

### Acknowledgment

The authors would like to express their gratitude to Ecocem for sponsoring this research. Additionally, the authors would like to acknowledge Tata Steel IJmuiden for providing the raw materials and conducting the quantitative XRD measurements.

### Appendix A. Supporting information

Supplementary data associated with this article can be found in the online version at doi:10.1016/j.conbuildmat.2025.143424.

# **Data Availability**

Data will be made available on request.

## References

- L. Poudyal, K. Adhikari, Environmental sustainability in cement industry: an integrated approach for Green and economical cement production, Resour. Environ. Sustain. 4 (December 2020) (2021) 100024, https://doi.org/10.1016/j. resenv.2021.100024.
- [2] N. Mohamad, K. Muthusamy, R. Embong, A. Kusbiantoro, M.H. Hashim, Environmental impact of cement production and solutions: a review, Mater. Today Proc. 48 (2021) 741–746, https://doi.org/10.1016/j.matpr.2021.02.212.
- [3] R.I. Cruz Juarez, S. Finnegan, The environmental impact of cement production in Europe: a holistic review of existing EPDs, Clean. Environ. Syst. 3 (August) (2021) 100053, https://doi.org/10.1016/j.cesys.2021.100053.
- [4] K.L. Scrivener, V.M. John, E.M. Gartner, Eco-efficient cements: potential economically viable solutions for a low-CO2 cement-based materials industry, Cem. Concr. Res 114 (February) (2018) 2–26, https://doi.org/10.1016/j. cemconres.2018.03.015.
- [5] H. Sun, J. Qian, Y. Yang, C. Fan, Y. Yue, Optimization of gypsum and slag contents in blended cement containing slag, Cem. Concr. Compos 112 (May) (2020) 103674, https://doi.org/10.1016/j.cemconcomp.2020.103674.
- [6] B. Lothenbach, K. Scrivener, R.D. Hooton, Supplementary cementitious materials, Cem. Concr. Res 41 (12) (2011) 1244–1256, https://doi.org/10.1016/j. cemconres.2010.12.001.
- [7] L. Black. Low Clinker Cement as a Sustainable Construction Material, Second Edi, Elsevier Ltd, 2016, https://doi.org/10.1016/b978-0-08-100370-1.00017-2.
- [8] I. Yuksel, Blast-furnace slag, Elsevier Ltd, 2018, https://doi.org/10.1016/B978-0-08-102156-9.00012-2.
- [9] C. Shi, Steel Slag—Its production, processing, characteristics, and cementitious properties, J. Mater. Civ. Eng. 16 (3) (2004) 230–236, https://doi.org/10.1061/ (asce)0899-1561(2004)16:3(230).
- [10] E. Belhadj, C. Diliberto, A. Lecomte, Characterization and activation of basic oxygen furnace slag, Cem. Concr. Compos 34 (1) (2012) 34–40, https://doi.org/ 10.1016/j.cemconcomp.2011.08.012.
- [11] T.S. Naidu, C.M. Sheridan, L.D. van Dyk, Basic oxygen furnace slag: review of current and potential uses, Min. Eng. 149 (January) (2020) 106234, https://doi. org/10.1016/j.mineng.2020.106234.
- [12] W.F. Santos, K. Schollbach, S. Melzer, S.R. van der Laan, H.J.H. Brouwers, Quantitative analysis and phase assemblage of basic oxygen furnace slag hydration, J. Hazard Mater. 450 (February) (2023) 131029, https://doi.org/ 10.1016/j.jhazmat.2023.131029.
- [13] A.S. Reddy, R.K. Pradhan, S. Chandra, Utilization of basic oxygen furnace (BOF) slag in the production of a hydraulic cement binder, Int J. Min. Process 79 (2) (2006) 98–105, https://doi.org/10.1016/j.minpro.2006.01.001.
   [14] K. Schollbach, M.J. Ahmed, S.R. Laan, The mineralogy of air granulated converter
- [14] K. Schollbach, M.J. Ahmed, S.R. Laan, The mineralogy of air granulated converte slag, Int. J. Ceram. Eng. Sci. 3 (1) (2021) 21–36, https://doi.org/10.1002/ ces2.10074.

- [15] M. Ma, H. Mehdizadeh, M.-Z. Guo, T.-C. Ling, Effect of direct carbonation routes of basic oxygen furnace slag (BOFS) on strength and hydration of blended cement paste, Constr. Build. Mater. 304 (August) (2021) 124628, https://doi.org/ 10.1016/j.conbuildmat.2021.124628.
- [16] N. Kabay, N. Miyan, H. Özkan, Basic oxygen furnace and ground granulated blast furnace slag based alkali-activated pastes: characterization and optimization, J. Clean. Prod. 327 (July) (2021), https://doi.org/10.1016/j.jclepro.2021.129483.
- [17] J.C.O. Zepper, S.R. van der Laan, K. Schollbach, H.J.H. Brouwers, Reactivity of BOF slag under autoclaving conditions, Constr. Build. Mater. 364 (ember 2022) (2023) 129957, https://doi.org/10.1016/j.conbuildmat.2022.129957.
- [18] A.M. Kaja, K. Schollbach, S. Melzer, S.R. van der Laan, H.J.H. Brouwers, Q. Yu, Hydration of potassium citrate-activated BOF slag, Cem. Concr. Res 140 (ember 2020) (2021) 106291, https://doi.org/10.1016/j.cemconres.2020.106291.
- [19] A.M. Kaja, S. Melzer, H.J.H. Brouwers, Q. Yu, On the optimization of BOF slag hydration kinetics, Cem. Concr. Compos 124 (January) (2021) 104262, https:// doi.org/10.1016/j.cemconcomp.2021.104262.
- [20] A. Kaja, Bouwstenen 308 Development of alternative cementitious binders and functionalized materials design, performance and durability, 2021. [Online]. Available: <a href="https://www.proefschriftmaken.nl">www.proefschriftmaken.nl</a>).
- [21] H. Zhu, et al., Effect of wet-grinding steel slag on the properties of portland cement: an activated method and rheology analysis, Constr. Build. Mater. 286 (2021) 122823, https://doi.org/10.1016/j.conbuildmat.2021.122823.
- [22] N. Elfami, H. Ez-zaki, A. Diouri, O. Sassi, A. Boukhari, Improvement of hydraulic and mechanical properties of dicalcium silicate by alkaline activation, Constr. Build. Mater. 247 (2020) 118589, https://doi.org/10.1016/j. conbuildmat.2020.118589.
- [23] M.J. Ahmed, K. Lambrechts, X. Ling, K. Schollbach, H.J.H. Brouwers, Effect of hydroxide, carbonate, and sulphate anions on the β-dicalcium silicate hydration rate, Cem. Concr. Res 173 (August) (2023) 107302, https://doi.org/10.1016/j. cemconres.2023.107302.
- [24] M.J. Ahmed, et al., V and cr substitution in dicalcium silicate under oxidizing and reducing conditions – synthesis, reactivity, and leaching behavior studies, J. Hazard Mater. 442 (May 2022) (2023) 130032, https://doi.org/10.1016/j. jhazmat.2022.130032.
- [25] Y.M. Kim, S.H. Hong, Influence of minor ions on the stability and hydration rates of β-dicalcium silicate, J. Am. Ceram. Soc. 87 (5) (2004) 900–905, https://doi.org/ 10.1111/j.1551-2916.2004.00900.x.
- [26] G. Kakali, S. Tsivilis, E. Aggeli, M. Bati, Hydration products of C3A, C3S and portland cement in the presence of CaCO3, Cem. Concr. Res 30 (7) (2000) 1073–1077, https://doi.org/10.1016/S0008-8846(00)00292-1.
- [27] M.J. Sánchez-Herrero, A. Fernández-Jiménez, A. Palomo, C3S and C2S hydration in the presence of Na2CO3 and Na2SO4, J. Am. Ceram. Soc. 100 (7) (2017) 3188–3198, https://doi.org/10.1111/jace.14855.
- [28] E. Berodier, K. Scrivener, Understanding the filler effect on the nucleation and growth of C-S-H, J. Am. Ceram. Soc. 97 (12) (2014) 3764–3773, https://doi.org/ 10.1111/jace.13177
- [29] Y. Briki, M. Zajac, M.Ben Haha, K. Scrivener, Impact of limestone fineness on cement hydration at early age, Cem. Concr. Res 147 (Sep. 2021) 106515, https:// doi.org/10.1016/J.CEMCONRES.2021.106515.
- [30] K. De Weerdt, M.Ben Haha, G. Le Saout, K.O. Kjellsen, H. Justnes, B. Lothenbach, Hydration mechanisms of ternary portland cements containing limestone powder and Fly ash, Cem. Concr. Res 41 (3) (2011) 279–291, https://doi.org/10.1016/j. cemeonres 2010 11 014
- [31] P. Hawkins, P. Tennis, and R. Detwiler, The Use of Limestone in Portland Cement: A State-of-the-Art Review, no. June 2003, 2019.
- [32] M. Hunger, An integral design concept for ecological self-compacting concrete, no. 2010, 10.6100/IR674188.
- [33] R. Snellings, et al., RILEM TC-238 SCM recommendation on hydration stoppage by solvent exchange for the study of hydrate assemblages, Mater. Struct. /Mater. Et. Constr. 51 (6) (2018), https://doi.org/10.1617/s11527-018-1298-5.
- [34] T.F. Scientific, Free Lime Determination in Clinker ARL 9900 Series XRF Spectrometer, pp. 1–4.
- [35] I. Vegas, A. Oleaga, V. García-Cortés, A. Santamaria, J.T. San-Jose, Assessment of steelmaking slags subjected to accelerated carbonation, Ain Shams Eng. J. 15 (7) (2024), https://doi.org/10.1016/j.asej.2024.102790.
- [36] H.S. Lee, H.S. Lim, M.A. Ismail, Quantitative evaluation of free CaO in electric furnace slag using the ethylene glycol method, Constr. Build. Mater. 131 (2017) 676–681, https://doi.org/10.1016/j.conbuildmat.2016.11.047.
- [37] Z. Jiang, J. Zepper, X. Ling, K. Schollbach, H.J.H. Brouwers, Potassium citrateactivated pure BOF slag-based mortars utilizing carbonated and autoclaved BOF slag aggregates, Cem. Concr. Compos 150 (April) (2024) 105564, https://doi.org/ 10.1016/j.cemconcomp.2024.105564.
- [38] and R. N. S. N.K. Katyal, 1\* S.C. Ahluwalia,† R. Parkash, No Titiウile, ペインクリニック学会治療指針 2, vol. 43, no. March, pp. 1–9, 1998
- [39] K.L. Scrivener, T. Füllmann, E. Gallucci, G. Walenta, E. Bermejo, Quantitative study of portland cement hydration by X-ray diffraction/rietveld analysis and independent methods, Cem. Concr. Res. 34 (9) (2004) 1541–1547, https://doi.org/ 10.1016/j.cemconres.2004.04.014.
- [40] J.C.O. Zepper, S.R. van der Laan, K. Schollbach, H.J.H. Brouwers, A bogue approach applied to basic oxygen furnace slag, Cem. Concr. Res. 175 (October 2023) (2024) 107344, https://doi.org/10.1016/j.cemconres.2023.107344.
- [41] W. Franco Santos, J.J. Botterweg, S. Chaves Figueiredo, K. Schollbach, S. van der Laan, H.J.H. Brouwers, Sodium oxalate activation of basic oxygen furnace slag for building materials, Resour. Conserv Recycl. 198 (January) (2023) 107174, https:// doi.org/10.1016/j.resconrec.2023.107174.

- [42] B. Lothenbach, G. Le Saout, E. Gallucci, K. Scrivener, Influence of limestone on the hydration of portland cements, Cem. Concr. Res. 38 (6) (2008) 848–860, https:// doi.org/10.1016/j.cemconres.2008.01.002.
- [43] A.M. Kaja, K. Schollbach, S. Melzer, S.R. van der Laan, H.J.H. Brouwers, Q. Yu, Hydration of potassium citrate-activated BOF slag, Cem. Concr. Res. 140 (ember 2020) (2021) 106291, https://doi.org/10.1016/j.cemconres.2020.106291.
- [44] A.M. Kaja, S. Melzer, H.J.H. Brouwers, Q. Yu, On the optimization of BOF slag hydration kinetics, Cem. Concr. Compos. 124 (January) (2021) 104262, https://doi.org/10.1016/j.cemconcomp.2021.104262.
- [45] I. Soroka, N. Stern, Calcareous fillers and the compressive strength of portland cement, Cem. Concr. Res. 6 (3) (1976) 367–376, https://doi.org/10.1016/0008-8846(76)00000-5
- [46] T. Oey, A. Kumar, J.W. Bullard, N. Neithalath, G. Sant, The filler effect: the influence of filler content and surface area on cementitious reaction rates, J. Am. Ceram. Soc. 96 (6) (2013) 1978–1990, https://doi.org/10.1111/jace.12264.
- [47] S.H. Kang, Y. Jeong, K.H. Tan, J. Moon, The use of limestone to replace physical filler of quartz powder in UHPFRC, Cem. Concr. Compos. 94 (April) (2018) 238–247, https://doi.org/10.1016/j.cemconcomp.2018.09.013.
- [48] P.C. Hewlett, Lea's Chemistry of Cement and Concrete, Lea's Chemistry of Cement and Concrete, pp. 1–1057, 2003, doi: 10.1016/B978-0-7506-6256-7.X5007-3.
- [49] K. Schollbach and S. van der Laan, Microstructure analysis with quantitative phase mapping using SEM-EDS and Phase Recognition and Characterization (PARC) Software: Applied to steelmaking slag, 2022. doi: 10.1515/9783110674941-003.
- [50] H. Kang, J. Lee, J.B. Park, J. Moon, Investigation on the Micro-Grinding induced crystallographic variations of nine different clinkers, Int J. Concr. Struct. Mater. 18 (1) (2024), https://doi.org/10.1186/s40069-024-00660-5.
- [51] J. Li, et al., Mechanical activation of medium basicity steel slag under dry condition for carbonation curing, J. Build. Eng. 50 (January) (2022) 104123, https://doi.org/10.1016/j.jobe.2022.104123.
- [52] K. Scrivener, R. Snellings, and B. Lothenbach, A Practical Guide to Microstructural Analysis of Cementitious Materials, 2018. doi: 10.1201/b19074.
- [53] B.Z. Dilnesa, B. Lothenbach, G. Renaudin, A. Wichser, D. Kulik, Synthesis and characterization of hydrogarnet Ca3(Al xFe1 - X)2(SiO4)y(OH) 4(3 - y), Cem. Concr. Res 59 (2014) 96–111, https://doi.org/10.1016/j.cemconres.2014.02.001.
- [54] R.L. Frost, A.W. Musumeci, T. Bostrom, M.O. Adebajo, M.L. Weier, W. Martens, Thermal decomposition of hydrotalcite with chromate, molybdate or sulphate in

- the interlayer, Thermochim. Acta 429 (2) (2005) 179–187, https://doi.org/10.1016/j.tca.2005.03.014.
- [55] Y. Zhang, G. Ye, Z. Yang, Pore size dependent connectivity and ionic transport in saturated cementitious materials, Constr. Build. Mater. 238 (2020) 117680, https://doi.org/10.1016/j.conbuildmat.2019.117680.
- [56] Z.L. Jiang, Y.J. Pan, J.F. Lu, Y.C. Wang, Pore structure characterization of cement paste by different experimental methods and its influence on permeability evaluation, Cem. Concr. Res. 159 (May) (2022) 106892, https://doi.org/10.1016/ i.cemconres.2022.106892.
- [57] P. Gao, G. Ye, J. Wei, and Q. Yu, Multi-scale simulation of capillary pores and gel pores in Portland cement paste, 14th International Congress on the Chemistry of Cement, Proceedings, vol. 31, no. 0, pp. 1–14, 2015, [Online]. Available: <a href="https://hdl.handle.net/1854/LU-6965135">https://hdl.handle.net/1854/LU-6965135</a>).
- [58] A.C.A. Muller et al., Bernhard Blümich Essential NMR, 2015. [Online]. Available: \(\langle \text{https://infoscience.epfl.ch/record/202011/files/EPFL\_TH6339.pdf\(\%\)0Ahttps: \(\langle \text{doi.org/10.1016/j.cemconres.2015.04.005}\).
- [59] L. Vernik, M. Bruno, C. Bovberg, Empirical relations between compressive strength and porosity of siliciclastic rocks, Int. J. Rock. Mech. Min. Sci. 30 (7) (1993) 677–680, https://doi.org/10.1016/0148-9062(93)90004-W.
- [60] H. Ahmadi Moghadam, A. Mirzaei, Z. Abedi Dehghi, The relation between porosity, hydration degree and compressive strength of portland cement pastes in the presence of aluminum chloride additive, Constr. Build. Mater. 250 (2020) 118884, https://doi.org/10.1016/j.conbuildmat.2020.118884.
- [61] A.M. Ramezanianpour, R.D. Hooton, A study on hydration, compressive strength, and porosity of Portland-limestone cement mixes containing SCMs, Cem. Concr. Compos 51 (2014) 1–13, https://doi.org/10.1016/j.cemconcomp.2014.03.006.
- [62] J. Péra, S. Husson, B. Guilhot, Influence of finely ground limestone on cement hydration, Cem. Concr. Compos 21 (2) (1999) 99–105, https://doi.org/10.1016/ S0958-9465(98)00020-1
- [63] X. Cong, R.J. Kirkpatrick, Effects of the temperature and relative humidity on the structure of CSH gel, Cem. Concr. Res 25 (6) (1995) 1237–1245, https://doi.org/ 10.1016/0008-8846(95)00116-T.
- [64] W. Kunther, strength of cementitious calcium silicate hydrate binders, vol. 2, pp. 17401–17412, 2017, doi: 10.1039/c7ta06104h.